AD-A075 480 MORGENTHALER (FREDERIC R) WELLESLEY MA F/G 9/5
THEORETICAL STUDIES OF MICROSTRIP ANTENNAS. VOLUME I. GENERAL D--ETC(U)
SEP 79 F R MORGENTHALER DOT-TS-15364
UNCLASSIFIED FAA-EM-79-11-1 NL

| OF |
AD
A075480

END
DATE
FILMED
11-79
DDC

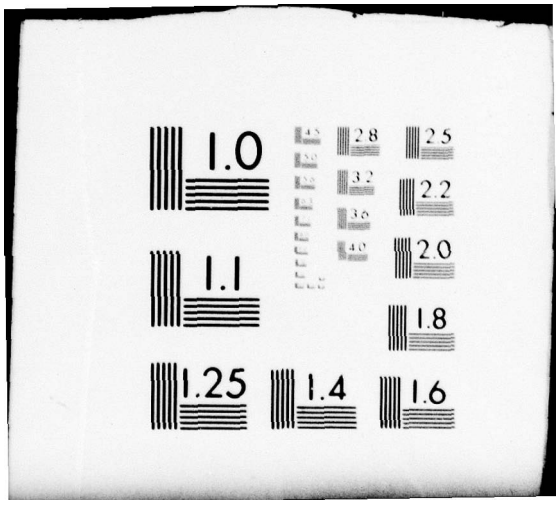
1.0
1.1
1.25
1.4
1.6
1.8
2.0
2.2
2.5
2.8
3.2
3.6
4.0

REPORT NO. FAA-EM-79-11, I

LEVEL II

AD A075480

THEORETICAL STUDIES OF MICROSTRIP ANTENNAS
Volume I: General Design Techniques and Analyses of Single and Coupled Elements

Frederic R. Morgenthaler
71 Abbott Road
Wellesley MA 02181

SEPTEMBER 1979

FINAL REPORT

Prepared for
U.S. DEPARTMENT OF TRANSPORTATION
FEDERAL AVIATION ADMINISTRATION
Office of Systems Engineering Management
Washington DC 20591

Technical Report Documentation Page

1. Report No.	2. Government Accession No.	3. Recipient's Catalog No.
FAA-EM-79-11-1, TSC	FAA-79-21-1	

4. Title and Subtitle
THEORETICAL STUDIES OF MICROSTRIP ANTENNAS
Volume I. General Design Techniques and Analyses of Single and Coupled Elements

5. Report Date
Sep[illegible]79

6. Performing Organization Code

7. Author(s)
Frederic R. Morgenthaler

8. Performing Organization Report No.
DOT-TSC-FAA-79-21-VOL-1

9. Performing Organization Name and Address
Frederic R. Morgenthaler*
71 Abbott Road
Wellesley MA 02181

10. Work Unit No. (TRAIS)
FA957/R9138

11. Contract or Grant No.
DOT-TS-15364-1

12. Sponsoring Agency Name and Address
U.S. Department of Transportation
Federal Aviation Administration
Office of Systems Engineering Management
Washington DC 20591

13. Type of Report and Period Covered
Final Report
Apr[illegible]1978-Jul[illegible]979

14. Sponsoring Agency Code

15. Supplementary Notes
*Under contract to: U.S. Department of Transportation
Research and Special Programs Administration
Transportation Systems Center
Cambridge MA 02142

16. Abstract

Volume I of Theoretical Studies of Microstrip Antennas deals with general design techniques and analyses of single and coupled radiating elements.

Specifically, we review and then employ an important equivalence theorem that allows a pair of vector potentials, $\vec{A}$ and $\vec{A}^*$ to be calculated from fields tangential to any surface enclosing all currents and charges.

These potentials serve to calculate the far fields, from which radiation conductance and pattern can be obtained.

For rectangular microstrip patch antennas, we develop novel approximations so as to include the effects of currents induced on the ground planes by fringing fields.

Coupling between two patches sharing the same substrate and ground plane, or else employing separate ones stacked one above the other, is also considered by means of a novel approximation that helps provide physical insight with respect to field patterns, coupling between patches and the like.

As an important by-product of this work, several new approximate formulas are obtained that very accurately predict the electrical characteristics of microstrip transmission lines of arbitrary width and substrate thickness when the dielectric constant of the substrate is also arbitrary.

Volume II of this report is devoted to the analysis and synthesis of multi-resonant elements with emphasis on dual-frequency operation of rectangular microstrip patch antennas with or without external matching networks.

17. Key Words	18. Distribution Statement
Microstrip Antennas Conformal Antennas Coupled Elements Mutual Impedance of Microstrip	DOCUMENT IS AVAILABLE TO THE PUBLIC THROUGH THE NATIONAL TECHNICAL INFORMATION SERVICE, SPRINGFIELD, VIRGINIA 22161

19. Security Classif. (of this report)	20. Security Classif. (of this page)	21. No. of Pages	22. Price
UNCLASSIFIED	UNCLASSIFIED	60	

Form DOT F 1700.7 (8-72) Reproduction of completed page authorized

411 420

PREFACE

Compact microwave antennas formed from resonant microstrip elements have recently attracted considerable attention because of their simplicity and conformability to shaped surfaces.

The Department of Transportation has been especially interested in this type of antenna for possible application with the Global Positioning System (GPS) and in aircraft satellite communications systems.

The work reported in both Volumes I and II of this document is aimed at providing a general theoretical framework useful for analyzing and/or synthesizing microstrip antennas and arrays. The work was completed and this report prepared by F. R. Morgenthaler under the direction of TSC Technical Monitor Leslie Klein.

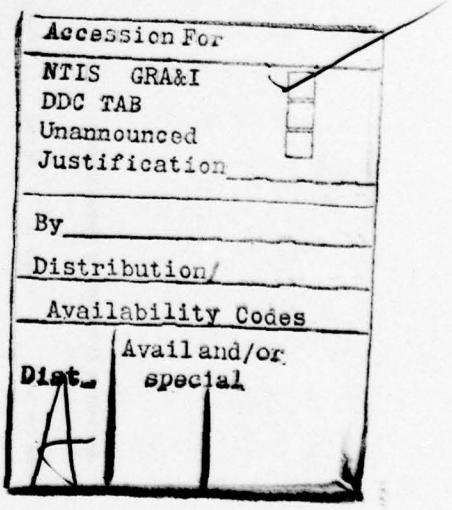

METRIC CONVERSION FACTORS

Approximate Conversions to Metric Measures

Symbol	When You Know	Multiply by	To Find	Symbol
	LENGTH			
in	inches	2.5	centimeters	cm
ft	feet	30	centimeters	cm
yd	yards	0.9	meters	m
mi	miles	1.6	kilometers	km
	AREA			
in^2	square inches	6.5	square centimeters	cm^2
ft^2	square feet	0.09	square meters	m^2
yd^2	square yards	0.8	square meters	m^2
mi^2	square miles	2.6	square kilometers	km^2
	acres	0.4	hectares	ha
	MASS (weight)			
oz	ounces	28	grams	g
lb	pounds	0.45	kilograms	kg
	short tons (2000 lb)	0.9	tonnes	t
	VOLUME			
tsp	teaspoons	5	milliliters	ml
tbsp	tablespoons	15	milliliters	ml
fl oz	fluid ounces	30	milliliters	ml
c	cups	0.24	liters	l
pt	pints	0.47	liters	l
qt	quarts	0.95	liters	l
gal	gallons	3.8	liters	l
ft^3	cubic feet	0.03	cubic meters	m^3
yd^3	cubic yards	0.76	cubic meters	m^3
	TEMPERATURE (exact)			
°F	Fahrenheit temperature	5/9 (after subtracting 32)	Celsius temperature	°C

Approximate Conversions from Metric Measures

Symbol	When You Know	Multiply by	To Find	Symbol
	LENGTH			
mm	millimeters	0.04	inches	in
cm	centimeters	0.4	inches	in
m	meters	3.3	feet	ft
m	meters	1.1	yards	yd
km	kilometers	0.6	miles	mi
	AREA			
cm^2	square centimeters	0.16	square inches	in^2
m^2	square meters	1.2	square yards	yd^2
km^2	square kilometers	0.4	square miles	mi^2
ha	hectares (10,000 m^2)	2.5	acres	
	MASS (weight)			
g	grams	0.035	ounces	oz
kg	kilograms	2.2	pounds	lb
t	tonnes (1000 kg)	1.1	short tons	
	VOLUME			
ml	milliliters	0.03	fluid ounces	fl oz
l	liters	2.1	pints	pt
l	liters	1.06	quarts	qt
l	liters	0.26	gallons	gal
m^3	cubic meters	35	cubic feet	ft^3
m^3	cubic meters	1.3	cubic yards	yd^3
	TEMPERATURE (exact)			
°C	Celsius temperature	9/5 (then add 32)	Fahrenheit temperature	°F

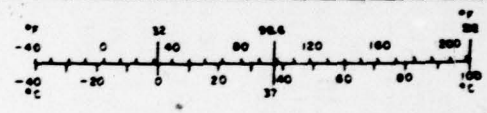

TABLE OF CONTENTS

LIST OF ILLUSTRATIONS

LIST OF TABLES

EXECUTIVE SUMMARY

Microwave antennas formed from resonant microstrip elements have recently attracted considerable attention because of their conformability to shaped surfaces, and their compactness and simplicity.

Although calculations based upon relatively simple theoretical models for the microstrip resonators appear to be in reasonable agreement with the experimental results available for comparison, it is of interest and benefit to critique the approximations that have been employed. This is so, because high performance from an array of elements often can be difficult to achieve unless higher-order terms pertinent to a single element, and mutual couplings among elements, are properly understood.

With this goal in mind, we first present a general approach that, in principle, would give a complete description of the radiation fields from any microstrip antenna consisting of one or more perfectly conducting metal patches, deposited upon the surface of a dielectric slab backed by a perfectly conducting metal sheet. Certain of the patches are presumed resonant at microwave frequencies of interest.

In particular, we review and then employ an important equivalence theorem that allows the radiation fields to be calculated from the components of electric and magnetic fields that are tangential to any surface enclosing all of the radiating currents and charges.

The approach used is first to find the modal structure within this surface (as effected by assumed fringing and radiation of the outer fields) and second to calculate these effects in a self-consistent manner.

Specifically, we develop formulas to estimate the strength of the electric charges and electric currents that are present on the top of the

structure consisting of coupled $\lambda/4$-resonant microstrip patches, the dielectric layer, and the ground plane, and the components at the radiation field arising from the currents.

In order to accomodate dual-frequency operation, Ball Aerospace Systems Division has developed a stacked element concept in which the smaller high-frequency patch is placed above the larger low-frequency one.

Because this is an important concept, we develop a transmission line model of this element with distributed coupling and solve for the excitations in both patches when the drive frequency corresponds to either the low or high resonance condition. We consider the cases of substrates both with dissimilar and with identical dielectric properties.

Throughout, emphasis is placed on developing equations describing both the near fields and the radiation fields; from the latter it is a simple matter to calculate radiation conductance, efficiency and pattern.

As an aid in these endeavors, we develop, in the Appendix A, a novel approximation that helps provide physical insight with respect to field patterns, coupling between patches and the like. For rectangular microstrip patches, the approximation allows simple analytic expressions to be obtained for the electric and magnetic field coupling coefficients between patches.

As an important by-product, several new approximate formulas are obtained that very accurately predict the characteristic impedance and phase velocity of microstrip transmission lines of arbitrary width when the dielectric constant of the substrate is also arbitrary. A comparison with other formulas established in the literature reveals that the relative accuracy is within 1-2 percent.

In an effort to highlight the fundamental formulation and facilitate use of the key results, especially important equations have been placed within a rectangular box outline.

1. INTRODUCTION

Microwave antennas formed from resonant microstrip elements have recently attracted considerable attention because of their conformability to shaped surfaces, and their compactness and simplicity.

The early work of Deschamps[1] was extended by Munson,[2] Itoh and Mittra,[3] Sanford,[4] Weinschel,[5] and more recently elaborated upon by Sanford and Klein,[6] Howell,[7] Agrawal et al.,[8] Derneryd,[9] Lo et al.,[10] James et al.[11] and others.

Although calculations based upon relatively simple theoretical models for the microstrip resonators appear to be in reasonable agreement with the experimental results available for comparison, it is of interest and benefit to critique the approximations that have been employed.

This is so because high performance from an array of elements often can be difficult to achieve unless higher-order terms pertinent to a single element and mutual couplings among elements are properly understood.

With this goal in mind, we first review a general approach that, in principle, would give an exact description of the radiation fields from any microstrip antenna array consisting of one or more perfectly conducting metal patches, such as that shown in Fig. 1, deposited upon the surface of a dielectric slab of finite extent and of thickness h, and backed by a perfectly conducting metal sheet. The sandwich structure is surrounded by free space.

The basic characteristics of microstrip lines are developed in Appendix A by novel approximations that help provide physical insight with respect to field patterns, coupling between lines and the like. For the present discussion, such details can be postponed.

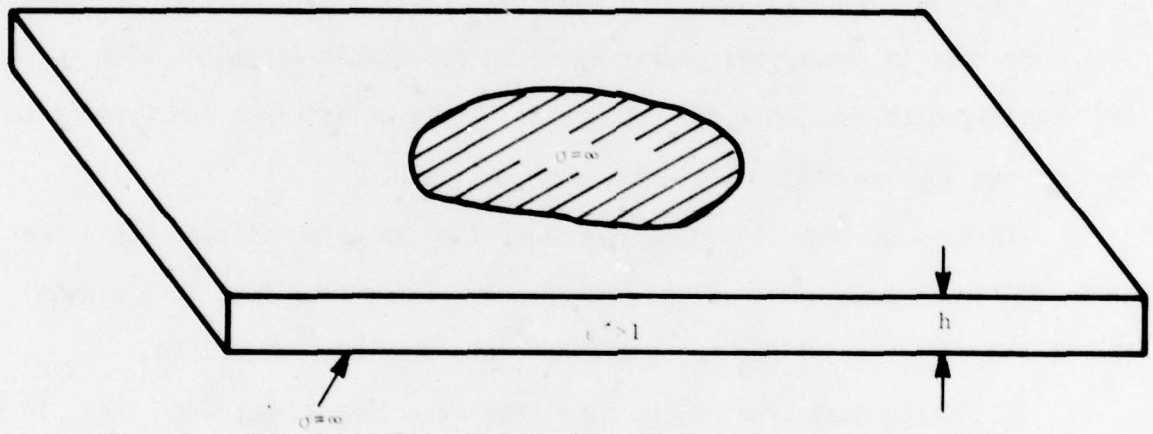

FIGURE 1. BASIC GEOMETRY OF MICROSTRIP PATCH

Although the actual sources of $\bar{E}$ and $\bar{H}$ consist of free electric currents flowing on the conducting surfaces, free charge resident upon them, and polarization current and charge on and within the dielectric slab, it is permissible to utilize fictitious magnetic current and charge densities ($\bar{J}^*$, ρ^*) (in addition to electric current and charge densities ($\bar{J}$, ρ)) to equivalently represent the sources at points external to them.

Following Chu[12], we express Maxwell's Eqs. in MKS units as

$$\nabla \times \bar{H} - \varepsilon_o \frac{\partial \bar{E}}{\partial t} = \bar{J} \tag{1}$$

$$\nabla \times \bar{E} + \mu_o \frac{\partial \bar{H}}{\partial t} = -\bar{J}^* \tag{2}$$

$$\varepsilon_o \nabla \cdot \bar{E} = \rho \tag{3}$$

$$\mu_o \nabla \cdot \bar{H} = \rho^*. \tag{4}$$

Since these equations are linear, it is convenient to resolve $\bar{E}$ and $\bar{H}$ into components $\bar{E}_1$, $\bar{H}_1$, due to $\bar{J}$, ρ alone and $\bar{E}_2$, $\bar{H}_2$ due to $\bar{J}^*$, ρ^* alone.

Then

$$\mu_o \bar{H}_1 = \nabla \times \bar{A} \tag{5a}$$

$$\bar{E}_1 = -\frac{\partial \bar{A}}{\partial t} - \nabla \psi \tag{5b}$$

where

$$A(\bar{r}_p, t) = -\int_v \frac{\mu_o \bar{J}(\bar{r}_Q, t - \frac{r_{Qp}}{c})}{4\pi r_{Qp}} dv_Q , \tag{6a}$$

$$\psi(\bar{r}_p, t) = -\int_v \frac{\rho(\bar{r}_Q, t - \frac{r_{Qp}}{c})}{4\pi\varepsilon_o r_{Qp}} dv_Q , \tag{6b}$$

$c = \frac{1}{\sqrt{\mu_o \varepsilon_o}}$ is the velocity of light in free space, r_{Qp} is the distance between the source point Q and field point P, and $\bar{r}_Q$ and $\bar{r}_p$ the respective vector distances as measured from a common origin.

Analogously,

$$\varepsilon_o \bar{E}_2 = \nabla \times \bar{A}^* \tag{7a}$$

$$\bar{H}_2 = \frac{\partial \bar{A}^*}{\partial t} - \nabla \psi^* \tag{7b}$$

where

$$\bar{A}^*(r_p,t) = \int_v \frac{\varepsilon_o \bar{J}^*(r_Q,\ t-\frac{r_{Qp}}{c})}{4\pi\ r_{Qp}}\, dv_Q \tag{8a}$$

and

$$\psi^*(\bar{r}_p,t) = -\int_v \frac{\rho^*(\bar{r}_Q,\ t-\frac{r_{Qp}}{c})}{4\pi\ r_{Qp}}\, dv_Q. \tag{8b}$$

At a surface of electromagnetic discontinuity at least one of the volume densities $\bar{J}$, ρ, $\bar{J}^*$, ρ^* is infinite and the respective boundary conditions associated with Eqs. (1) - (4) are

$$\bar{n}\times(\bar{H}_{(1)} - \bar{H}_{(2)}) = \bar{K} \tag{9a}$$

$$\bar{n}\times(\bar{E}_{(1)} - \bar{E}_{(2)}) = -\bar{K}^* \tag{9b}$$

$$\varepsilon_o \bar{n}_o(\bar{E}_{(1)} - \bar{E}_{(2)}) = \sigma_s \tag{10a}$$

$$\mu_o \bar{n}\ (\bar{H}_{(1)} - \bar{H}_{(2)}) = \sigma_s^* \tag{10b}$$

where the direction of the normal $\bar{n}$ with respect to the surface and the definition of sides (1) and (2) are given in Fig. (2). Note that $\bar{H}_{(i)}$ should not be confused with $\bar{H}_i$; the number in parenthesis refers to the side of the surface. Thus $\bar{H}_{1(2)}$ refers to the field of Eq. (5a) on side (2) of the surface of discontinuity.

Here $\bar{K}$ and $\bar{K}^*$ are, respectively, electric and "magnetic" surface current densities and σ_s and σ_s^* are, respectively, electric and "magnetic" surface charge densities.

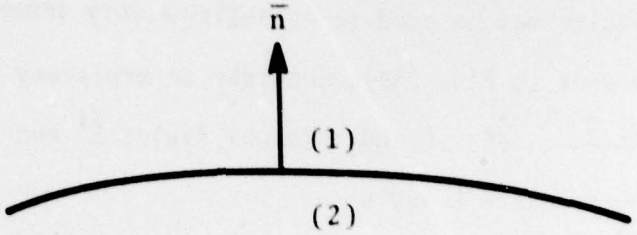

Conventions pertaining at a surface of discontinuity. The unit normal vector $\bar{n}$ is directed from side (2) toward side (1).

FIGURE 2. SURFACE OF ELECTROMAGNETIC DISCONTINUITY

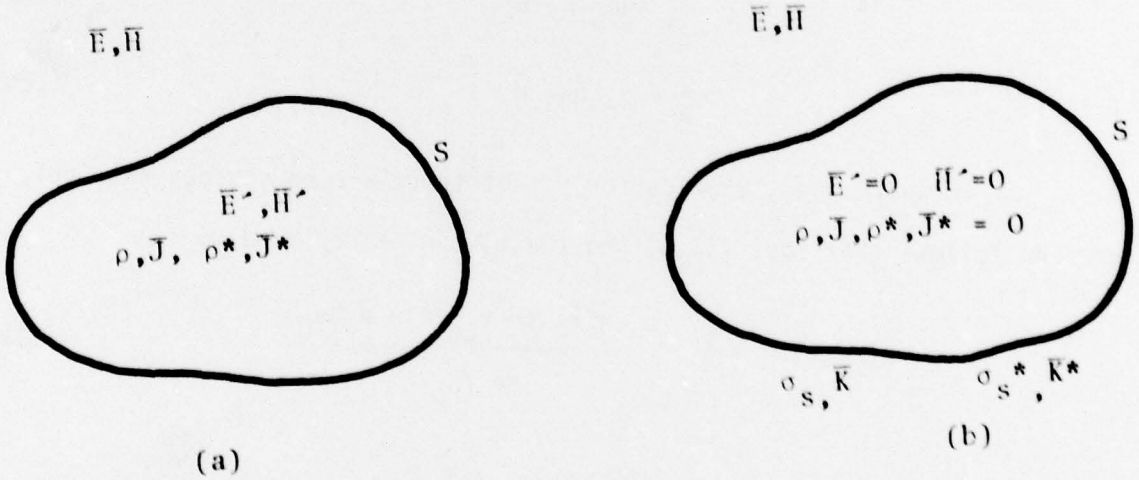

In a; the volume sources $\bar{J}$, ρ, $\bar{J}^*$, ρ^* within the closed surface S create $\bar{E}$, $\bar{H}$ outside. In b, appropriate sources $\bar{K}$, σ_s, $\bar{K}^*$, σ_s^* located on the surface create the identical fields outside, but E = 0 and H = 0 within the surface.

FIGURE 3. EQUIVALENCE PRINCIPLE FOR ELECTROMAGNETIC FIELDS

These results may be used to establish a very important equivalence principle. With reference to Fig. (3a), consider an arbitrary closed surface S containing sources $\bar{J}$, ρ, $\bar{J}^*$, ρ^* and internal fields $\bar{E}^i$ and $\bar{H}^i$. The fields external to the surface are $\bar{E}$ and $\bar{H}$.

In this connection, consider Fig.(3b) in which an identically shaped surface encloses a field and source free region, except that surface currents and charges exist on the surface. The fields external to the surface are assumed to be identical to those in Fig. (3a).

Since the normal vector points outward, $\bar{E}_{(2)} = 0$, $\bar{H}_{(2)} = 0$ and the required surface sources are

$$\bar{K} = \bar{n} \times \bar{H} \tag{11a}$$

$$-\bar{K}^* = \bar{n} \times \bar{E} \tag{11b}$$

$$\sigma_s = \varepsilon_o \bar{n} \cdot \bar{E} \tag{12a}$$

$$\sigma_s^* = \mu_o \bar{n} \cdot \bar{H}. \tag{12b}$$

As is well known, provided only that there are no sources enternal, it therefore follows that Eqs. (5a,b) and (8a,b) can be replaced by

$$\bar{A}(\bar{r}_p,t) = + \oint_s \frac{\mu_o \bar{H}(\bar{r}_Q, t - r_{Qp}/c) \times \bar{n}\, da_Q}{4\pi\, r_{Qp}} \tag{13a}$$

$$\psi(\bar{r}_p,t) = - \oint_s \frac{\bar{E}(\bar{r}_Q, t - r_{Qp}/c) \cdot \bar{n}\, da_Q}{4\pi\, r_{Qp}} \tag{13b}$$

$$\bar{A}^*(\bar{r}_p,t) = + \oint_s \frac{\varepsilon_o \bar{E}(\bar{r}_Q, t - r_{Qp}/c) \times \bar{n}\, da_Q}{4\pi r_{Qp}} \tag{14a}$$

and $$\psi^*(r_p,t) = -\oint_S \frac{\bar{H}(\bar{r}_Q, t - r_{Qp}/c)\cdot n\, da_Q}{4\pi r_{Qp}} \quad . \tag{14b}$$

The element da_Q is the scalar differential area at any point Q that lies on the surface S.

Notice that for complex harmonic time dependence, employing retarded time

$$\exp j\omega(t - (\frac{r_{Qp}}{c})) = \exp(-jkr_{Qp})\exp(j\omega t)$$

where $k = \omega/c$. In this case, the complex vector potentials for sinusoidal steady state frequency ω are

$$\bar{A}(\bar{r}_p) = \oint_S \frac{\mu_o e^{-jkr_{Qp}} H_Q(\bar{r}_Q) \times d\bar{a}_Q}{4\pi\, r_{Qp}} \tag{15a}$$

and

$$\bar{A}^*(\bar{r}_p) = \oint_S \frac{\varepsilon_o e^{-jkr_{Qp}} \bar{E}_Q(\bar{r}_Q) \times d\bar{a}_Q}{4\pi r_{Qp}} \quad . \tag{15b}$$

It is not necessary to calculate the scalar potentials from the normal components of the fields, because, in free space, the total fields are expressible as

$$\bar{E} = -j\, c/k \nabla \times (\nabla \times \bar{A}) + 1/\varepsilon_o \nabla \times \bar{A}^* \tag{16a}$$

$$\bar{H} = j\, c/k \nabla \times (\nabla \times \bar{A}^*) + 1/\mu_o \nabla \times \bar{A}. \tag{16b}$$

This is a consequence of their having to satisfy the complex form of the free space Maxwell Equations.

SUMMARY REMARKS

Knowledge of the $\bar{E}$ and $\bar{H}$ fields tangential to any surface, S, enclosing all currents and charges allows $\bar{A}$ and $\bar{A}^*$ to be calculated; these in turn allow the fields to be obtained at any point external to S. When that point is far from the antenna, even fairly crude approximations of the fields on S will allow the radiation fields, radiation conductance and pattern to be calculated in a straight-forward manner.

This information, when fed back, allows the near fields to be calculated with improved accuracy.

We turn next to the important case of the rectangular microstrip patch radiator - essentially a $\lambda/4$ strip transmission line radiating from the open circuit end of the resonator. [We employ reasonable approximations to derive $\bar{A}$ and $\bar{A}^*$]. The element is driven at an appropriate distance from the short circuit end where the impedance allows a favorable match to the input microstrip transmission line.

2. RECTANGULAR MICROSTRIP PATCH RADIATOR

Consider a single rectangular patch of width w and length L shorted to the ground plane at z = 0 as shown in Fig. 4a, b. Assume first that the dielectric constant of the supporting slab is unity.

If the resonator is excited at the frequency for which L is approximately $\lambda/4$, the mode pattern will resemble that shown in the figure. In particular, if $h/\lambda << 1$, the fields between the plates will be quasi-TEM and the fringing fields at the edges will be comparatively weak.

The equivalent circuit of the transmission line will then be as shown in Fig. 5 where G_0 and B_0 are in general frequency dependent when $\varepsilon' > 1$ (because then exact TEM modes are not possible). For the present $\varepsilon' = 1$, therefore $B_0 = 0$ and the frequency independent G_0 includes the effects of lateral fringing (Fig. 4b). The lumped capacitance C_f models the fringing at the open circuit (shown in Fig. 4a). The conductance G_r represents the power radiated from the structure or else lost due to conversion to surface wave excitations.[13]

Since normally the resonator is high Q, G_r may be neglected when solving for the resonant frequencies.

Transverse resonance (or what is the same, continuity of voltage and current) requires

$$Y_0 \cot kL \simeq \omega C_f . \tag{17}$$

For $\omega C_f / Y_0 << 1$, the principal mode satisfies $kL \simeq \pi/2 + \Delta$

$$\tan \Delta \simeq \Delta \simeq - \frac{\omega C_f}{Y_0} . \tag{18}$$

Defining $kL^{eff} = \pi/2$ and using

$$k = \omega \sqrt{L'C'} \tag{19}$$

and

$$Y_0 = \sqrt{\frac{C'}{L'}} \tag{20}$$

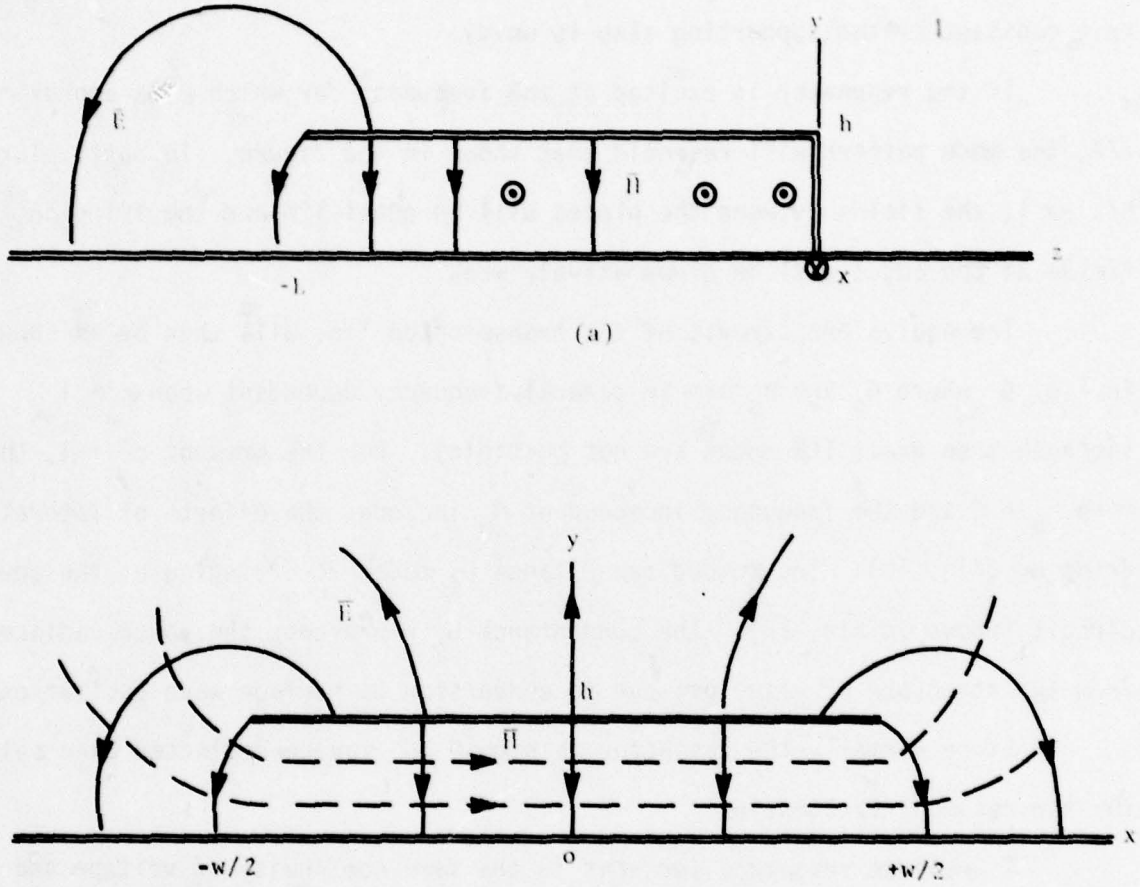

$\bar{E}$ and $\bar{H}$ field patterns associated with a resonant rectangular microstrip patch of width w and length L = $\lambda/4$. An rf short exists at z = 0; the three other sides are open.

FIGURE 4. $\bar{E}$ AND $\bar{H}$ FIELD PATTERNS ASSOCIATED WITH A RESONANT RECTANGULAR MICROSTRIP PATCH OF WIDTH w AND LENGTH L = $\lambda/4$

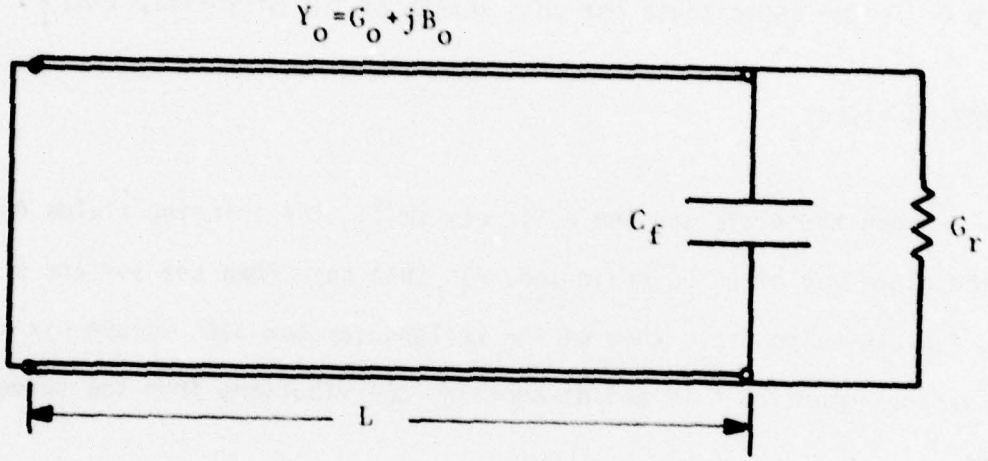

An equivalent transmission line model corresponding to wave propagation directed along the z-coordinate of Fig. 4.

FIGURE 5. AN EQUIVALENT TRANSMISSION LINE MODEL

gives

$$L^{eff} = L + \frac{C_f}{C'} \tag{21}$$

where C' is the capacitance per unit length of the microstrip line.

RADIATION FIELDS

When the plate spacing h is very small, the fringing fields outside of the plate may often be neglected. In this case then the surface S of Eqs. (15) corresponds to that of the rectangular box with volume L x W x H. The vector potential $\bar{A} \simeq 0$ and $\bar{A}^*$ contains contributions from the three open sides.

For $z = -L$ $\quad |x| < W/2 \quad 0 \leq y \leq h,$

$$\bar{E} \simeq \bar{i}_y E_o \tag{22a}$$

and applying Eq. (15b) gives

$$\bar{A}^*_{\text{front face}} = \bar{i}_x \frac{\varepsilon_o E_o whe^{-jkr}}{4\pi r} \frac{\sin(\frac{kwx}{2r})}{(\frac{kwx}{2r})} \left(\frac{e^{j\frac{kh}{r}y} - 1}{j\frac{kh}{r}y}\right) e^{-jkL\frac{z}{r}} . \tag{22b}$$

For the sides $x = \pm W/2$, $0 \leq y < h$, $-L \leq z \leq 0$

$$\bar{E} \simeq \bar{i}_y E_o \sin Kz \tag{23a}$$

and again applying Eq. (15b) gives

$$\bar{A}^*_{\text{sides}} = \bar{i}_z \frac{\varepsilon_o E_o Lhe^{-jkr}}{2\pi r} \sin(\frac{kwx}{2r}) \left(\frac{e^{j\frac{khy}{r}} - 1}{j\frac{kh}{r}y}\right) \frac{\frac{kL}{r} ze^{-j\frac{kLz}{r}} + j\frac{\pi}{2}}{(\frac{\pi}{2})^2 - (\frac{kL}{r}z)^2} . \tag{23b}$$

Because $kh \ll 1$, the factors involving y are approximately unity.

The principal effect of the fringing is not to alter $\bar{A}^*$ but rather to create a vector potential $\bar{A}$ that is also z-directed.

The vector potential $\bar{A}$ arising from the surface currents due to the fringing field can be estimated by integrating the tangential $\bar{H}$-field along the path shown in Fig. 6 for a strip of width dz. For a point P in the far field region, Eq. (15a) has only a single component that may be approximated as

$$A_z = \frac{\mu_o}{4\pi}\frac{e^{-jkr}}{r}\int_{\xi}\int_{z'=-L}^{0} d\xi dz' H_{tan}(\xi,z') e^{jk[\sin\theta(\cos\phi x' + \sin\phi y')\, d\xi dz' + \cos\theta z']} \tag{24}$$

where ξ(either x' or y') is the surface coordinate along the path.

Assuming a TEM field of the form

$$H_{tan}(\xi,z') = -H_{\xi}(\xi)\sin\left(\frac{\pi}{2L}z'\right)$$

and both $kh \ll 1$ and $kS \ll 1$, Eq. (24) can be further approximated as

$$A_z \simeq \frac{\mu_o}{4\pi}\frac{e^{-jkr}}{r}\frac{L}{2}F(\theta)\left\{\int_{-\infty}^{-w/2-\Delta} H_x(x)e^{jk\sin\theta\cos\phi x}\,dx + \int_{-w/2+\Delta}^{w/2-\Delta} H_x(x)e^{jk\sin\theta\cos\phi x}\,dx + \int_{w/2+\Delta}^{\infty} H_x(x)e^{jk\sin\theta\cos\phi x}\,dx + e^{-jk\,w/2\sin\theta\cos\phi}\int_{a'}^{b'} H_t(\xi)d\xi + e^{jk\,w/2\sin\theta\cos\phi}\int_{b}^{a} H_t(\xi)d\xi\right\} \tag{25}$$

where

$$F(\theta) = \frac{\pi}{(kL\cos\theta)^2 - (\pi/2)^2} + \frac{e^{j(kL\cos\theta+\pi/2)}}{kL\cos\theta+\pi/2} - \frac{e^{-j(kL\cos\theta-\pi/2)}}{kL\cos\theta-\pi/2} \tag{26}$$

For $h/w \ll 1$, the values of $H_x(x)$ for $|x| < w/2 - \Delta$ and $|x| > w/2 + \Delta$ can be approximated with the help of a vector potential A_z that has the same form as

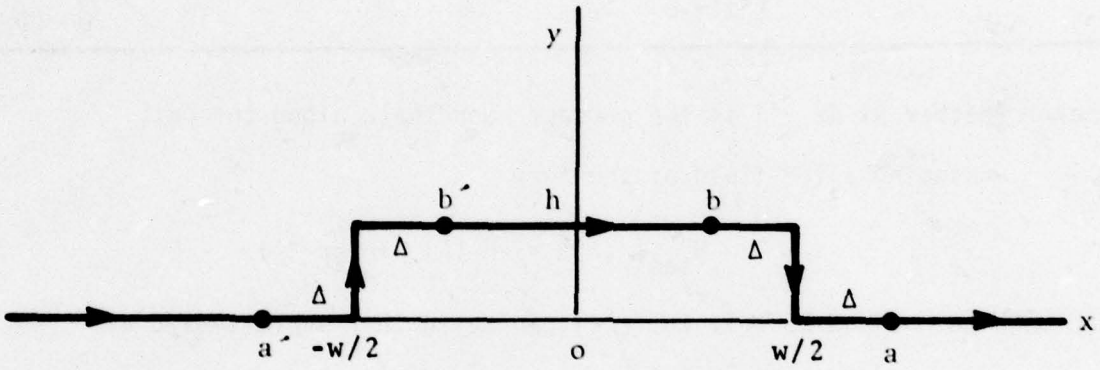

The contour of integration associated with the ξ coordinate of Eq. (24).

FIGURE 6. THE CONTOUR OF INTEGRATION

Eqs. (A-1) and (A-2) of the Appendix, (except with $\varepsilon' = 1$).

The result is

$$H_x(x) \simeq \begin{cases} \dfrac{-H_o hw}{hw + \pi[(w/2)^2 - x^2]} & |x| < w/2 - \Delta \\ \dfrac{H_o hw}{hw + \pi[x^2 - (w/2)^2} & |x| > w/2 + \Delta \end{cases} \tag{27}$$

where H_o is the amplitude in the uniform field region (inside of the parallel plates). These expressions allow the first three integrals on the right hand side of Eq. (25) to be evaluated analytically.

These expressions are, of course, not accurate too near the edges of microstrip patch and we dare not let $\Delta = 0$.

However, since w/h>>1, we can safely employ near each edge, a vector potential of the form given in Eq. (A-4) . In particular with,

$$A_z = \frac{H_o h}{\pi} v \tag{28a}$$

and

$$\int \bar{H} \cdot \bar{ds} = \frac{H_o h}{\pi} u, \qquad (x = \frac{w}{2}, y = h) \tag{28b}$$

the conjugate potential functions u and v satisfy

$$\frac{\pi(x - w/2)}{h} = e^u \cos v + u + 1 \tag{29a}$$

and

$$\frac{\pi y}{h} = e^u \sin v + v \tag{29b}$$

near the right hand edge (x = w/2).

The last integral on the right hand side of Eq. (25) can be evaluated as

$$\int_b^a H\xi(\xi)\, d\xi = \frac{H_o h}{\pi} (u_a - u_b) \tag{30}$$

where from Eqs. (20a,b),

$$e^{u_a} + u_a + 1 = \frac{\pi\Delta}{h} = e^{u_b} - u_b - 1 \quad . \tag{31}$$

For convenience in evaluating the first three integrals, we choose $\Delta = h/\pi$ and find $2(u_a - u_b) \simeq -1.09$. From symmetry consideration,

$$\int_{a'}^{b'} H_\xi(\xi)\, d\xi = \int_{b}^{a} H_\xi(\xi)\, d\xi \ ,$$

therefore the complete analytic approximation of Eq. (25) may be written as

$$A_z \simeq \frac{\mu_o H_o(hL) e^{-jkr}}{4\pi r} F(\theta) \left\{ \frac{2}{\pi} \int_{2h/\pi}^{\infty} \frac{\sin(k\sin\theta\cos\phi\nu)}{\nu}\, d\nu \right.$$

$$\left. \times \sin\left(\frac{kw}{2}\sin\theta\cos\phi\right) - \frac{1.09}{2}\cos\left(\frac{kw}{2}\sin\theta\cos\phi\right) \right\} . \tag{32}$$

Because $kh/\pi \ll 1$, the lower limit of the integral can be set equal to zero and since $\int_0^\infty \frac{\sin a\xi}{\xi} d\xi = \pi/2 \frac{a}{|a|}$, the final result is

$$A_z \simeq \frac{\mu_o H_o(hL)}{4\pi r} e^{-jkr} F(\theta) \left[\sin\left| \frac{kw}{2}\sin\theta\cos\phi \right| - .55\left(\cos\frac{kw}{2}\sin\theta\cos\phi\right) \right] \tag{33}$$

where $F(\theta)$ is given by Eq. (26).

Of course, H_o and E_o are related by $E_o/H_o = \sqrt{\frac{\mu_o}{\varepsilon'_{eff}\varepsilon_o}}$ with ε'_{eff} calculated from Eqs. (A-9) and (A-10).

Notice that this estimate of A_z assumes that the ground plane extends many wavelengths and also that the transverse field pattern is Laplacian in nature (a consequence of the TEM approximation that neglects any z-components of the field generated by the fringing at the open front face).

Eqs. (16) can now be employed to calculate the radiation fields, radiated power and G_r. The latter value can be used to modify Eq. (17) if necessary.

3. COUPLING BETWEEN STACKED MICROSTRIP PATCHES

In order to accomodate dual-frequency operation, Ball Aerospace Systems Division has developed the stacked element concept[4] in which a smaller, high-frequency patch is placed above the larger, low-frequency patch. In this section, we develop a transmission line model with distributed coupling and solve for the excitation in both patches when the drive frequency corresponds to either the low or high resonance condition. We consider the cases of substrates both with dissimilar and with identical dielectric properties.

A cross-section of the stacked micro-patch geometry is shown in Fig. 7a and represents any x-y plane in the range $0<z<L_1$. The two dielectric slabs need not be identical. A section through the y-z plane is given in Fig. 7b. A transmission line model for the z-variation of the fields is shown in Fig. 7c. Notice that coupling region extends over the length of the upper plate, $(0 \leq z \leq L)$.

3.1 TRANSMISSION LINE MODEL

The transmission line equations governing the voltages $V_1(z)$ and $V_2(z)$, measured with respect to the bottom ground plane, and the currents $i_1(z)$ and $i_2(z)$, representing respectively the <u>total</u> currents on the conducting patches, are for quasi-TEM modes, well-approximated by

$$-\frac{\partial i_1}{\partial z} = C'_{11}\frac{\partial v_1}{\partial t} + C'_{12}\frac{\partial v_2}{\partial t} \tag{34a}$$

$$-\frac{\partial v_1}{\partial z} = L'_{11}\frac{\partial i_1}{\partial t} + L'_{12}\frac{\partial i_2}{\partial t} \tag{34b}$$

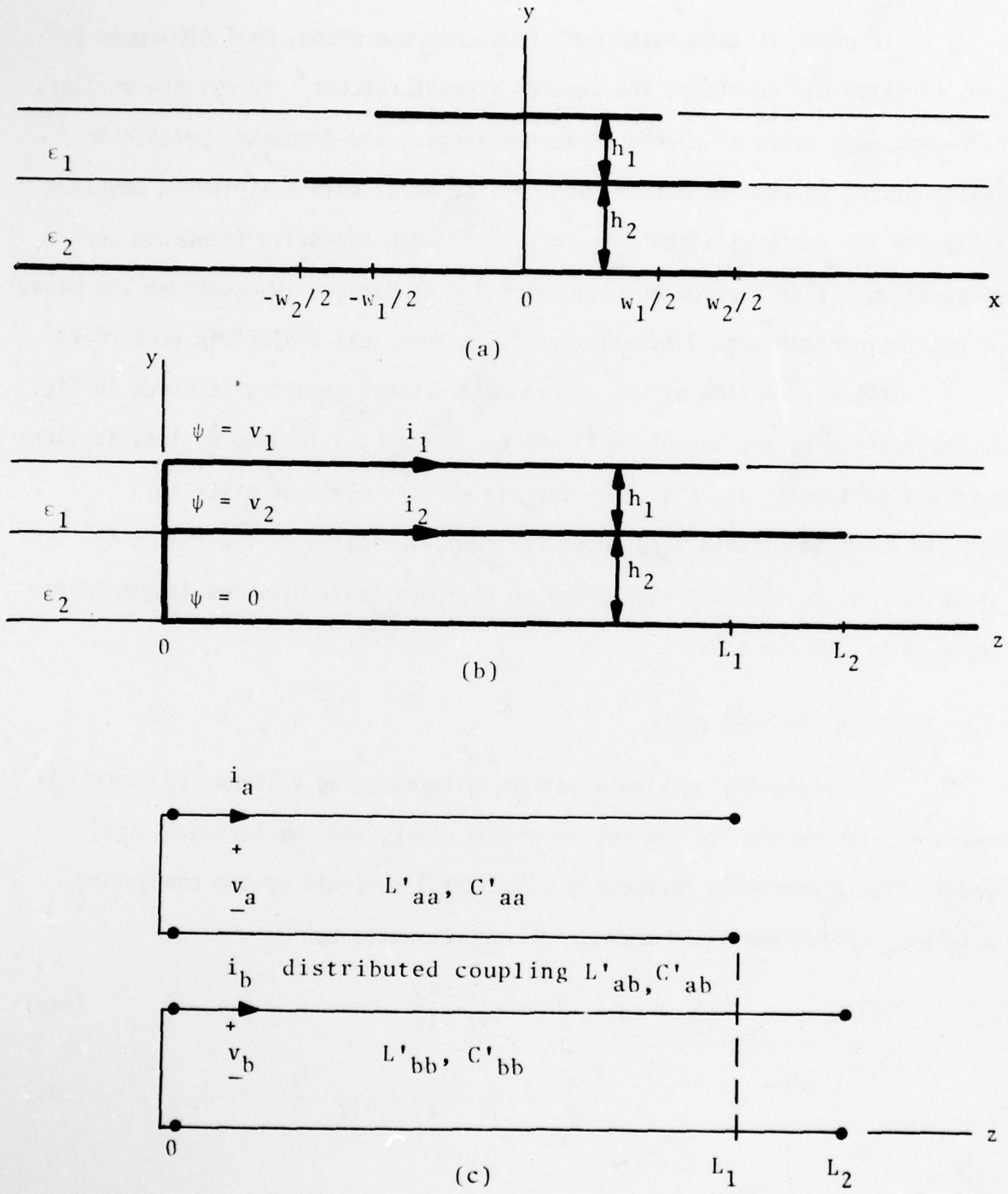

The high frequency microstrip patch is placed above the low frequency radiator as shown in a and b. The equivalent transmission line circuit is shown in c.

FIGURE 7. STACKED ELEMENTS FOR DUAL-FREQUENCY COVERAGE

and

$$-\frac{\partial i_2}{\partial z} = C'_{12}\frac{\partial v_1}{\partial t} + C'_{22}\frac{\partial v_2}{\partial t} \tag{35a}$$

$$-\frac{\partial v_2}{\partial z} = L'_{12}\frac{\partial i_1}{\partial t} + L'_{22}\frac{\partial i_2}{\partial t} \tag{35b}$$

where $C'_{12} \leq 0$ and $L'_{12} \geq 0$.

Because these voltages and currents contain contributions from the fields under both patches even if the fringing fields are zero, the coupling terms are always non zero.

It is therefore preferable to define new variables, namely

$$v_a = v_1 - v_2 \tag{36a}$$

$$v_b = v_2 \tag{36b}$$

and

$$i_a = i_1 \tag{37a}$$

$$i_b = i_2 + i_1. \tag{37b}$$

The coupled-transmission lines for these choices are shown in Fig. 7c; the governing equations are

$$-\frac{\partial i_a}{\partial z} = C'_{aa}\frac{\partial v_a}{\partial t} + C'_{ab}\frac{\partial v_b}{\partial t} \tag{38a}$$

$$-\frac{\partial v_a}{\partial z} = L'_{aa}\frac{\partial i_a}{\partial t} + L'_{ab}\frac{\partial i_b}{\partial t} \tag{38b}$$

and

$$-\frac{\partial i_b}{\partial z} = C'_{ab}\frac{\partial v_a}{\partial t} + C'_{bb}\frac{\partial v_b}{\partial t} \tag{39a}$$

$$-\frac{\partial v_b}{\partial z} = L'_{ab}\frac{\partial i_a}{\partial t} + L'_{bb}\frac{\partial i_b}{\partial t} \tag{39b}$$

where the capacitances and inductances per unit length (along z) are

$$C'_{aa} = C'_{11} \simeq \frac{\varepsilon_1 w_1}{h_1} \tag{40a}$$

$$C'_{bb} = C'_{11} + C'_{22} + 2C'_{12} \simeq \frac{\varepsilon_2 w_2}{h_2} \tag{40b}$$

$$C'_{ab} = C'_{11} + C'_{12} \equiv k_e \sqrt{C'_{aa} C'_{bb}} > 0 \tag{40c}$$

and

$$L'_{aa} = L'_{11} + L'_{22} - 2L'_{12} \simeq \mu_o \frac{h_1}{w_1} \tag{41a}$$

$$L'_{bb} = L'_{22} \simeq \mu_o \frac{h_2}{w_2} \tag{41b}$$

$$L'_{ab} = L'_{12} - L'_{22} \equiv k_m \sqrt{L'_{aa} L'_{bb}} > 0. \tag{41c}$$

The electric and magnetic coupling coeffients, respectively k_e and k_m are both less than unity; if fringing is neglected, they both vanish and the lines are uncoupled.

Because the mode Qs are moderate to high, it is reasonable to neglect the radiation from the open circuited ends of the lines, this implies that the mode voltages and currents are in time-quadrature.

We therefore take

$$v_{a,b} = V_{a,b}(z) \sin\omega t \tag{42a}$$

$$i_{a,b} = I_{a,b}(z) \cos\omega t \tag{42b}$$

and reduce Eqs. (38) and (39) to

$$-\frac{dIa}{dz} = \frac{\varepsilon_1 w_1}{h_1} \omega V_a + \omega C'_{ab} V_b \tag{43a}$$

$$\frac{dVa}{dz} = \mu_o \frac{h_1}{w_1} \omega I_a + \omega L'_{ab} I_b \tag{43b}$$

$$-\frac{dI_b}{dz} = \frac{\varepsilon_2 w_2}{h_2}\,\omega\, V_b + \omega C'_{ab}\, V_a \qquad (44a)$$

$$\frac{dV_b}{d_z} = \mu_o \frac{h_2}{W_2}\,\omega I_b + \omega L'_{ab}\, I_a \ . \qquad (44b)$$

These in turn may be combined to yield

$$\frac{d^2 Va}{dz^2} + \omega^2(\mu_o\varepsilon_1 + L'_{ab}C'_{ab})V_a = -\omega^2(\mu_o \frac{h_1}{W_1} C'_{ab} + \varepsilon_2 \frac{w_2}{h_2} L'_{ab})\, V_b \qquad (45a)$$

$$\frac{d^2 V_b}{dz^2} + \omega^2(\mu_o\varepsilon_2 + L'_{ab}\, C'_{ab})V_b = -\omega^2(\mu_o \frac{h_2}{W_2} C'_{ab} + \varepsilon_1 \frac{w_1}{h_1} L'_{ab})\, V_a. \qquad (45b)$$

If the two dielectric constants are the same, $\varepsilon_1 = \varepsilon_2 = \varepsilon$, the uncoupled phase velocities of the two plate transmission lines are equal and coupling is enhanced.

In general, the spatial voltages along the two lines are found from Eq. (45) to be

$$V_a = A \sin k_1 z + \frac{k_I^2}{k_2^2 - k_a^2}\, B \sin k_2 z \qquad (v \le z \le L_1) \qquad (46a)$$

and

$$V_b = \begin{cases} \dfrac{k_{II}^2}{k_1^2 - k_b^2}\, A \sin k_1 z + B \sin k_2 z & (0 \le z \le L_1) \\ C \cos k_b (L_2 - z) & (L_1 \le z \le L_2) \ . \end{cases} \qquad (46b)$$

No mutual coupling is assumed to exist over the interval $L_1 \le z \le L_2$. Here, because the coupling is weak,

$$k_a^2 = \omega^2(\mu_o\varepsilon_1 + L'_{ab}\, C'_{ab}) \simeq \omega^2\mu_o\varepsilon_1 \qquad (47a)$$

$$k_b^2 = \omega^2(\mu_o\varepsilon_2 + L'_{ab}\, C'_{ab}) \simeq \omega^2\mu_o\varepsilon_2 \qquad (47b)$$

$$k_I^2 = \omega^2 \mu_o \sqrt{\frac{h_2 w_1}{h_1 w_2}}\, \sqrt{\varepsilon_1}\,(\sqrt{\varepsilon_2}\, k_e + \sqrt{\varepsilon_1}\, k_m) \qquad (48a)$$

$$k_{II}^2 = \omega^2 \mu_o \sqrt{\frac{h_1 w_2}{h_2 w_1}}\, \sqrt{\varepsilon_2}\,(\varepsilon_1\, k_e + \sqrt{\varepsilon_2}\, k_m) \qquad (48b)$$

and $k_{1,2}$ are the roots of

$$(k^2 - k_a^2)\,(k^2 - k_b^2) = k_I^2\, k_{II}^2 \quad . \qquad (49)$$

The associated currents are from Eqs. (43b) and (44b),

$$I_a = \frac{1}{\omega(1 - k_m^2)}\, \frac{w_1 w_2}{\mu_o^2\, h_1 h_2} \left(\mu_o \frac{h_2}{w_2} \frac{dV_a}{dz} - L'_{ab} \frac{dV_b}{dz}\right) \qquad (50a)$$

and

$$I_b = \frac{1}{\omega(1 - k_m^2)}\, \frac{w_1 w_2}{\mu_o^2\, h_1 h_2} \left(\mu_o \frac{h_1}{w_1} \frac{dV_b}{dz} - L'_{ab} \frac{dV_a}{dz}\right) . \qquad (50b)$$

When boundary conditions are imposed (continuity of V_b and I_b at $z = L_1$ and $I_a(L_1) = I_b(L_2) = 0$), the coefficients A, B and C are constrained to

$$\left(\mu_o \frac{h_2}{w_2} - L'_{ab} \frac{k_{II}^2}{k_1^2 - k_b^2}\right) k_1 A \cos k_1 L_1 + \left(\mu_o \frac{h_2}{w_2} \frac{k_I^2}{k_2^2 - k_a^2} - L'_{ab}\right) k_2 B \cos k_2 L_1 = 0 \qquad (51a)$$

$$\frac{k_{II}^2}{k_1^2 - k_v^2} A \sin k_1 L_1 + B \sin k_2 L_1 = C \cos k_b (L_2 - L_1) \qquad (51b)$$

and

$$\left(-L'_{ab} + \mu_o \frac{h_1}{w_1} \frac{k_{II}^2}{k_1^2 - k_b^2}\right) k_1 A \cos k_1 L_1 + \left(-L'_{ab} \frac{k_I^2}{k_2^2 - k_a^2} + \mu_o \frac{h_1}{w_1}\right) k_2 B \cos k_2 L_1 = \mu_o \frac{h_2}{w_2}\, k_b C \sin k_b (L_2 - L_1). \qquad (51c)$$

In order to establish the resonance conditions, the determinant formed from Eq. (51) is set equal to zero and the characteristic frequencies must be found.

As expected "$\lambda/4$ - resonances" exist for either $k_a L_1 \simeq \pi/2$ or $k_b L_2 \simeq \pi/2$. If the two frequencies ω_1 and ω_2 are too closely spaced, appreciable excitation can occur on both lines. We next consider the unwanted excitation on line b when line a is driven at its frequency, and vice versa. Two situations are of interest. In the first instance $\varepsilon_1 \neq \varepsilon_2$ and the phase velocities of the two lines are unequal; in the second, $\varepsilon_1 = \varepsilon_2 = \varepsilon$ and the velocities are also equal.

3.2 UNEQUAL PHASE VELOCITIES

When $\varepsilon_1 \neq \varepsilon_2$ and the coupling is weak

$$k_1 \simeq k_a + \frac{k_I^2 k_{II}^2}{2k_a(k_a^2 - k_b^2)} \tag{52a}$$

and

$$k_2 \simeq k_b + \frac{k_I^2 k_{II}^2}{2k_b(k_b^2 - k_a^2)} \quad . \tag{52b}$$

If line 1 is driven at its resonance (ω_1),

$$V_a \sim V_o \sin k_a z \tag{53a}$$

and

$$V_b(L_2) \simeq V_o \sqrt{\frac{h_1 w_2}{h_2 w_1}} \; \frac{\sqrt{\varepsilon_2}(\sqrt{\varepsilon_1}\, k_e + \sqrt{\varepsilon_2}\, k_m)}{(\varepsilon_1 - \varepsilon_2)} \; \frac{\cos\left(\frac{\varepsilon_2}{\varepsilon_1}\,\frac{\pi}{2}\right)}{\cos\left(\frac{\omega_1}{\omega_2}\,\frac{\pi}{2}\right)} \; . \tag{53b}$$

If line 2 is driven at its resonance (ω_2),

$$V_b \sim V_o \sin k_b z \tag{54a}$$

and

$$V_a(L_1) = V_o \sqrt{\frac{h_2 w_1}{h_1 w_2}} \; \frac{\sqrt{\varepsilon_1}(\sqrt{\varepsilon_2}\, k_e + \sqrt{\varepsilon_1}\, k_m)}{\varepsilon_1 - \varepsilon_2} \left[\sqrt{\frac{\varepsilon_2}{\varepsilon_1}} \; \frac{\cos\left(\sqrt{\frac{\varepsilon_2}{\varepsilon_1}}\,\frac{\omega_2}{\omega_1}\,\frac{\pi}{2}\right)}{\cos\left(\frac{\omega_2}{\omega_1}\,\frac{\pi}{2}\right)} - \sin\left(\sqrt{\frac{\varepsilon_2}{\varepsilon_1}}\,\frac{\omega_2}{\omega_1}\,\frac{\pi}{2}\right) \right] . \tag{54b}$$

3.3 EQUAL PHASE VELOCITIES

When $\varepsilon_1 = \varepsilon_2 = \varepsilon$, $k_a = k_b = k_o$ and

$$k_+^2 - k_o^2 = k_o^2 - k_-^2 = k_I\, k_{II} \tag{55}$$

or since the coupling is weak,

$$k_1 = k_+ = k_o + \Delta k \tag{56a}$$

$$k_2 = k \;\; = k_o - \Delta k \tag{56b}$$

with

$$\frac{\Delta k}{k_o} \simeq \frac{k_I k_{II}}{2k_o^2} = \frac{k_e + k_m}{2} << 1 \quad . \tag{56c}$$

In this case,

$$V_a = \left(A + \frac{k_I^2}{k^2 - k_o^2}\, B\right) \sin k_o z + \left(A - \frac{k_I^2}{k^2 - k_o^2}\, B\right) \Delta k\; z \cos k_o z \qquad 0 \le z \le L_1 \tag{57a}$$

and

$$V_b = \begin{cases} \left(\dfrac{k_{II}^2}{k_+^2 - k_o^2}\, A + B\right) \sin k_o z + \left(\dfrac{k_{II}^2}{k_+^2 - k_o^2}\, A - B\right) \Delta k z \cos k_o z & \\ \qquad\qquad 0 \le z \le L_1 \quad . & \\ C \cos k_o (L_2 - z) \qquad L_1 \le z \le L_2 & \end{cases} \tag{57b}$$

If line # 1 is driven so that

$$V_a \simeq V_o \sin k_o z \tag{58a}$$

it follows that

$$V_b(L_2) \simeq V_o\, \frac{\sqrt{\dfrac{h_1 w_2}{h_2 w_1}}\, (k_e + k_m)\, \dfrac{\pi}{4}}{\cos\left(\dfrac{\omega_1}{\omega_2}\, \dfrac{\pi}{2}\right)} \quad . \tag{58b}$$

If line # 2 is driven so that

$$V_b \simeq V_o \sin k_o z \tag{59a}$$

it follows that

$$V_a(L_1) \simeq \left[\frac{\frac{\pi}{2} \frac{\omega_2}{\omega_1}}{\cos\left(\frac{\pi}{2} \frac{\omega_2}{\omega_1}\right)} - \sin\left(\frac{\pi}{2} \frac{\omega_2}{\omega_1}\right) \right] \frac{k_e + k_m}{2} \sqrt{\frac{h_2 w_1}{h_1 w_2}} V_o \quad . \tag{59b}$$

Notice that if $\omega_1 \simeq \omega_2$, the denominators of Eqs. (53b), (54b), (58b) and (59b) will all tend to vanish leading to large amplitudes of voltage in the undriven lines.

Even neglecting loss as we have done, the true amplitudes will not become infinite when the more exact Eqs. (51) are considered. The crucial point however, is that the approximate results allow comparisons to be made among the cases considered and indicate how close the dual resonances can become before appreciable mode excitation in the undriven patch creates problems with the radiation characteristics of the composite antenna.

The critical factor is $\left|\cos \frac{\pi}{2} \frac{\omega_2}{\omega_1}\right|^{-1}$. Notice that for dual-frequency applications of current interest, namely the Global Positioning System (GPS) and Aerosat , the values of ω_2/ω_1 are respectively 1.3 and 1.07. Consequently, the respective values of $\left|\cos\left(\frac{\pi}{2} \frac{\omega_2}{\omega_1}\right)\right|^{-1}$ are 2.2 and 9.1.

4. CONCLUSIONS AND RECOMMENDATIONS

The work described in Volume I of this report allows predictions to be made regarding the non ideal behavior of rectangular microstrip patch antennas including the effects of ground plane currents and intra-element coupling due to fringing electric and magnetic fields.

It would be helpful, and the principal investigator recommends, that a sufficient number of detailed calculations be carried out for single and multiple-elements (with a variety of substrates) to establish the range of validity of the formulas developed here by comparing the results with presently available data.

It is likely that some new experiments would have to be carried out to allow a full comparison to be made.

After such validation, the design of antenna arrays with exacting pattern requirements should be attempted and compared with coordinated experiments.

APPENDIX A

MICROSTRIP FORMULAS BASED UPON NOVEL APPROXIMATIONS

A.1 INTRODUCTION

The basic microstrip geometry given in Fig. A1 consists of a dielectric sheet of thickness h and dielectric constant $\varepsilon' \geq 1$, clad on its lower surface (y=-h) with a conducting sheet and on its upper surface with a conducting strip of width w. Free space exists above the dielectric (y>0).

Although many workers[14-17] have described and given approximate expressions for the characteristic impedance and phase velocity of the quasi-TEM mode that propagates on microstrip it is appropriate to re-examine the subject and we do so in this appendix.

It is not that the previous work is inadequate for computation of the characteristic impedance and wave velocity of microstrip, but rather that we wish to develop (if possible) a simple approximation that will allow calculations of field distributions which in turn can be used to find electric and/or magnetic coupling between microstrip patches. Fortunately, we are able to achieve our goal and as a by product several new formulas are developed that should also prove useful in microstrip transmission line analysis. In particular, the new formulas for $h/w \geq 1$ and arbitrary value of dielectric constant are particularly simple and $Z_0(h/w)$ can be inverted to yield $h/w(Z_0)$. The latter form facilitates the synthesis of lines of prescribed impedance.

A.2 APPROXIMATE POTENTIAL FUNCTION

With reference to Fig. A1, and assuming $h/w \ll 1$, consider the function

$$\psi/v_o \simeq \frac{wh + \varepsilon' \sqrt{\left[x^2 + y^2 - (\frac{w}{2})^2\right]^2 + (wy)^2}\ T(x,y)}{wh + \pi\varepsilon' \sqrt{\left[x^2 + y^2 - (\frac{w}{2})^2\right]^2 + (wy)^2}} \qquad y \geq 0, \tag{A1a}$$

where

$$T(x,y) = \tan^{-1}\left(\frac{y}{x-w/2}\right) - \tan^{-1}\left(\frac{y}{x+w/2}\right) \tag{A1b}$$

and

$$\psi/v_o \simeq \begin{cases} \dfrac{y+h}{h} & |x| \leq w/2 \qquad -h \leq y \leq 0. \quad \text{(A2a)} \\ \dfrac{w(y+h)}{wh + \pi\varepsilon'[x^2 - (\frac{w}{2})^2]} & |x| \geq w/2 \quad \text{(A2b)} \end{cases}$$

First, it should be noted tht this function was <u>not</u> derived in the usual. Instead, it was developed as an interpolation based upon physical intuition. Second, notice that, if considered as a potential function, Eqs. (1) and (2) satisfy exactly the boundary condition of Fig. A1, namely $\psi(y=-h) = 0$, $\psi(|x|<w/2,\ y = 0) = V_o$ and

$$\frac{\partial\psi}{\partial y}(|x| \geq w/2,\ y = 0+) = \varepsilon' \frac{\partial\psi}{\partial y}(|x| \geq w/2,\ y = 0-).$$

Third, notice that for $[x^2 + y^2 - (\frac{w}{2})^2]^2 + (wy)^2 >> w^2d^2$ and $y>0$,

$\psi \simeq \frac{V_o}{\pi} T(x,y)$ which is a Laplacian function, as is

$$\psi(\sqrt{x^2 + y^2} << w \quad , y \geq 0) \simeq V_o(1 - \frac{4}{\pi w} y)$$

and

$$\psi(|x|<w/2,\ y<0) = V_o(1 + y/h).$$

Although $\psi(|x|>w/2,\ y<0)$ is <u>not</u> exactly Laplacian, the discrepancies vanish for large $|x|$. Therefore, Eq. (A1) is a comparatively simple formula that interpolates between asymptotically correct limits.

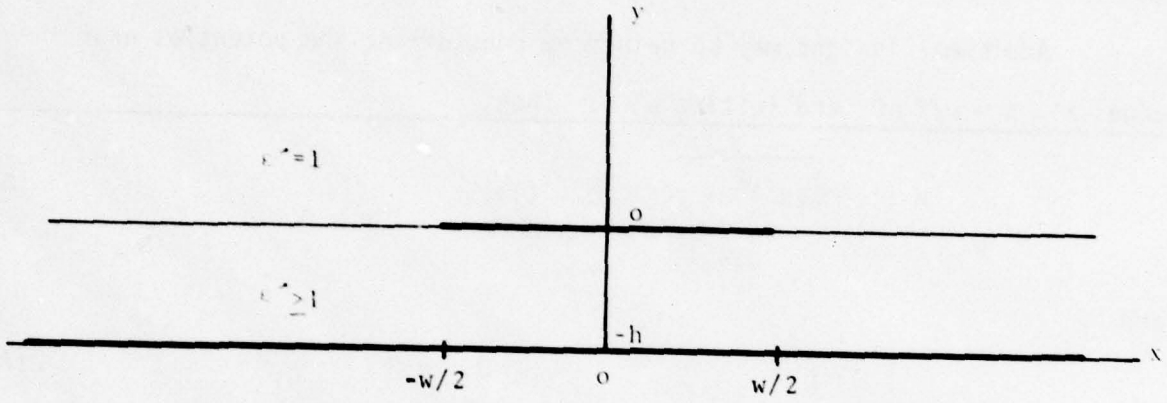

The conducting plane (y = -h) and strip (y = 0, $|x| \leq w/2$) are assumed to have infinite conductivity and zero thickness; the slab of dielectric constant $\varepsilon' \geq 1$ and thickness h is assumed lossless.

FIGURE A-1. MICROSTRIP GEOMETRY SHOWN IN CROSS SECTION

The principal errors are associated with the region near the plate edges because this approximation does not allow the E-field to become infinite at these locations. This defect is important only when h/w is not small compared to unity.

Additional insight may be gained by considering the potential near the edge $x' = x - w/2 \simeq 0$. and letting $w \to \infty$. Then,

$$\psi/V_o \simeq \frac{h + \varepsilon' \sqrt{(x')^2 + y^2} \quad \tan^{-1}\left(\frac{y}{x'}\right)}{h + \pi\varepsilon' \sqrt{(x')^2 + y^2}} \qquad y \geq 0 \tag{A3a}$$

and

$$\psi/V_o \simeq \begin{cases} \dfrac{y + h}{h} & x' \leq 0 \\ \dfrac{y + h}{h + \pi\varepsilon' x'} & x' \geq 0 \end{cases} \qquad -h < y \geq 0 \; . \tag{A3b}$$

When $\varepsilon' = 1$, the exact potential may be found by the method of conformal transformation; the well known result is

$$\frac{\pi x}{h} = \frac{\pi(y + h)}{h} - v \cot v + \ell n \left[\frac{\frac{\pi(y + h)}{h} - v}{\sin v}\right] + 1 \tag{A4}$$

where $v = \frac{\pi\psi}{V_o}$.

A comparison between the approximate and exact formulae is given in Fig. A-2. Notice that the E field strength, proportional to the spacing between equipotentials, is given quite accurately except very close to the edge of the upper plate $(x = 0, y = 0)$. Also notice that the approximate formula (and also physical reasoning) indicates that the extent of the fringing is reduced as ε' is increased. This fact suggests that the approximate formula becomes more accurate in such cases since the regions of non-Laplacian interpolation, between those that are asymptotically correct, are reduced.

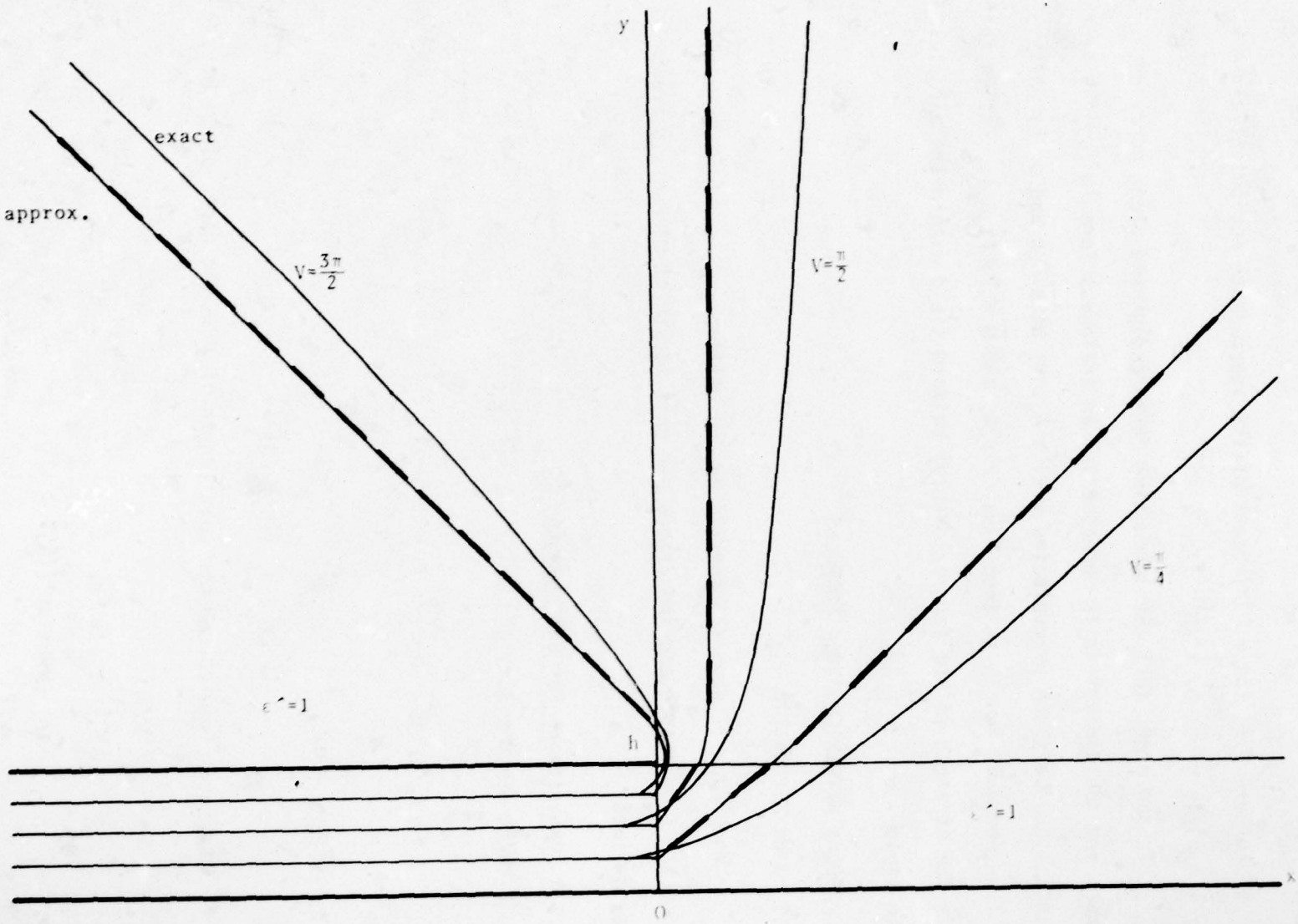

Comparison of exact and approximate equipotentials calculated near x=w/z for the structure of Fig. A-1, when $w \to \infty$ and $\varepsilon' = 1$.

FIGURE A-2. COMPARISON OF EXACT AND APPROXIMATE EQUIPOTENTIALS

For example, the x' intercept of the approximate equipotential $\psi = V_o/2$ (for $y = 0$) is given by $x'/h = 1/\pi\varepsilon'$.

In the event that the conducting strip and ground plane carry dc current and the dielectric is nonmagnetic, an analogous formula for the vector potential can be given by replacing ψ with A_z, V_o with $H_o h$ and ε' by unity. The flux per unit length is then $\text{Flux}' = \mu_o A_z$ and $\bar{H} = \nabla \times (\bar{i}_z A_z)$. Notice that H_o is the strength of the (approximately) uniform field within the parallel plate region.

A.3 APPROXIMATE MICROSTRIP FORMULAS

A.3.1 Wide Microstrip

When $h/w \ll 1$, Eqs. (1) and (2) can be utilized approximately to calculate the capacitance and inductance per unit length of microstrip transmission lines.

A.3.1.1 Capacitance Per Unit Length

For $|x| < w/2$, $y = 0+$

$$\psi \simeq V_o \left[1 - \frac{\varepsilon' w y}{wh + \varepsilon\pi \left[\left(\frac{w}{2}\right)^2 - x^2\right]}\right] . \tag{A5a}$$

For $|x| < w/2$, $y = 0-$

$$\psi \simeq V_o \, (1 + y/h) . \tag{A5b}$$

The total <u>free</u> charge per unit length of z on the upper plate is therefore

$$Q' = \varepsilon_o \int_{-w/2}^{w/2} \frac{V_o \varepsilon' w \, dx}{wh + \pi\varepsilon'\left[\left(\frac{w}{2}\right)^2 - x^2\right]} + \varepsilon \int_{-w/2}^{+w/2} V_o h \, dx \tag{A6a}$$

and

$$C' = \frac{Q'}{V_o} = \frac{\varepsilon w}{h} + \frac{2\varepsilon_o \frac{w}{\pi}}{\sqrt{\left(\frac{w}{2}\right)^2 + \frac{wh}{\pi\varepsilon'}}} \tanh^{-1}\left(\frac{w/2}{\sqrt{\left(\frac{w}{2}\right)^2 + \frac{wh}{\pi\varepsilon'}}}\right) . \tag{A6b}$$

A.3.1.2. Inductance Per Unit Length

When the conducting strip carries a dc current I, the magnetic vector potential is z-directed with $A_z/(H_o h)$ replacing ψ/V_o and setting $\varepsilon' = 1$ in Eqs. (A-1) and (A-2). Then, since $\bar{H} = \nabla x(\bar{i}_z A_z)$, it follows that

$$I = \int_{-w/2}^{+w/2} [H_x(x,y=0) - H_x(x,y=0+)]\, dx \quad . \tag{A-7a}$$

Because the magnetic flux per unit length (along z) is $Flux' = \mu_o A_z$, the inductance per unit length L' is given by

$$L' = \frac{Flux'}{I} = \frac{\mu_o}{\frac{w}{h} + \frac{2w/\pi}{\left(\frac{w}{2}\right)^2 + \frac{wh}{\pi}} \tanh^{-1} \frac{2w/\pi}{\left(\frac{w}{2}\right)^2 + \frac{wh}{\pi}}} \quad . \tag{A-7b}$$

It is convenient to define a dimensionless parameter $\sigma = 4h/\pi W$. In terms of σ, Eqs. (A-7b) and (A-6b) become respectively

$$L'/\mu_o = \frac{\pi/4}{\frac{1}{\sigma} + \frac{1}{\sqrt{1+\sigma}} \tanh^{-1}\left(\frac{1}{\sqrt{1+\sigma}}\right)} \tag{A-8a}$$

and

$$\varepsilon_o/C' = \frac{\pi/4}{\frac{\varepsilon'}{\sigma} + \frac{1}{\sqrt{1+\sigma/\varepsilon'}} \tanh^{-1}\left(\frac{1}{\sqrt{1+\sigma/\varepsilon'}}\right)} \quad . \tag{A-8b}$$

Although these expressions are expected to be valid only when $h/w \ll 1$, we have found, empirically, that their validity can be extended over the entire range $h/w \leq 1$ by adding simple correction terms to the denominators of Eqs. A-8a, b which then become

$$L'/\mu_o = \frac{\pi/4}{\frac{1}{\sigma}.15 + \frac{1}{\sigma} + \frac{1}{\sqrt{1+\sigma}} \tanh^{-1}\left(\frac{1}{\sqrt{1+\sigma}}\right)} \qquad \text{(A-9a)}$$

and

$$\varepsilon_o/C' = \frac{\pi/4}{(\varepsilon')^{\frac{\varepsilon'-1}{\varepsilon'+1}}\,\sigma.15 + \frac{\varepsilon'}{\sigma} + \frac{1}{\sqrt{1+\sigma/\varepsilon'}} \tanh^{-1}\left(\frac{1}{\sqrt{1+\sigma/\varepsilon'}}\right)} . \qquad \text{(A-9b)}$$

If the dispersion induced by the non-TEM components of the true transmission line fields is neglected, certainly valid for $h/w \ll 1$, the phase and group velocities are given by $v \simeq c/\sqrt{\varepsilon'}_{eff}$ where

$$\varepsilon'_{eff} = c\sqrt{L'C'} \quad . \qquad \text{(A-10)}$$

The appropriate characteristic impedance is found from

$$Z_o = \sqrt{\frac{L'}{C'}} \quad . \qquad \text{(A-11)}$$

The accuracy of our approximations can be assessed by comparing the values of ε'_{eff} and $Z_o\,\varepsilon_o$ with the accurate values of Wheeler[13] and Hammerstad[15] that were developed by a combination of exact and quasi-empirical means. This comparison is given in Table 1 for both Eqs. (A-8a,b) and Eqs. (A-9a,b).

A.3.2 NARROW MICROSTRIP

When $w/h < 1$, the approximate formulas given above are not valid and it is instructive to consider an alternative approach based upon the method of images.

First assume $\varepsilon' = 1$, and note that the charge distribution of Fig. (A-3)a produces the proper electric field in the half space $y \geq 0$ provided $Q'(x)$ and its image cause the strip $y = h$, $|x| \leq w/2$ to be an equipotential of value V. If w/h is sufficiently small, the effect of the image charges

TABLE A-1 WIDE MICROSTRIP

	ε'_{eff}				$Z_o/\sqrt{\frac{\mu_o}{\varepsilon_o}}$				
h/w	Morgenthaler (A-8a,b)(A-9a,b)		Wheeler Hammerstad		Morgenthaler (A-8a,b)(A-9a,b)		Wheeler Hammerstad		
.01	1		1		.0096	.0096	.0096	.0096	
.05	1		1		.0443	.0427	.0429	.0427	
.10	1		1		.0826	.0767	.0765	.0765	$\varepsilon' = 1$
.50	1		1		.3284	.2362	.2350	.2348	
1.00	1		1		.5972	.3339	.3350	.3346	
.10	1.4033	1.4017	1.4050	1.4044	.0069	.0068	.0069	.0068	
.05	1.3808	1.3723	1.3785	1.3767	.0321	.0311	.0311	.0310	
.10	1.3657	1.3497	1.3579	1.3554	.0605	.0568	.0564	.0567	$\varepsilon' = 2$
.50	1.3419	1.284	1.3030	1.303	.2448	.1839	.1804	.1824	
1.00	1.3485	1.2439	1.2837	1.2834	.4429	.2663	.2610	.2607	
.01	2.2067	2.2039	2.2111	2.2113	.0044	.0044	.0044	.0043	
.05	2.1427	2.1286	2.1385	2.1404	.0207	.0201	.0200	.0199	
.10	2.0963	2.071	2.0816	2.0853	.0394	.0370	.0368	.0368	$\varepsilon' = 5$
.50	1.9938	1.9183	1.9308	1.9380	.1647	.1231	.1217	.1223	
1.00	1.9901	1.8718	1.8799	1.8854	.3001	.1784	.1782	.1775	
.01	3.1142	3.1110	3.1215	3.1228	.0031	.0031	.0031	.0031	
.05	3.0068	2.9920	3.0024	3.0096	.0147	.0143	.0143	.0142	
.10	2.9262	2.9019	2.9080	2.9213	.0282	.0264	.0263	.0263	$\varepsilon' = 10$
.50	2.7230	2.6795	2.6612	2.6834	.1206	.0881	.0883	.0884	
1.00	2.6886	2.6348	2.5792	2.5977	.2221	.1267	.1299	.1288	

on the form of Q'(x) is negligible and the latter can be found from the solution of a single charged strip. That potential is proportional to v (taken as zero on the strip) where

$$\frac{x^2}{1+\sinh^2 v} + \frac{(y-h)^2}{\sinh^2 v} = \left(\frac{w}{2}\right)^2 \qquad \text{(A-12)}$$

The potential that is the superposition of a pair of such terms (the second due to the image) is

$$\psi = \frac{-Q'}{2\pi\varepsilon_o} \sinh^{-1} \sqrt{\frac{\left[\left(\frac{2x}{w}\right)^2 + 4\left(\frac{y-h}{w}\right)^2 - 1\right] + \sqrt{\left[\left(\frac{2x}{w}\right)^2 + 4\left(\frac{y-h}{w}\right)^2 - 1\right]}}{2}}$$
$$+\frac{Q'}{2\pi\varepsilon_o} \sinh^{-1} \sqrt{\frac{\left[\left(\frac{2x}{w}\right)^2 + 4\left(\frac{y+h}{w}\right)^2 - 1\right] + \sqrt{\left[\left(\frac{2x}{w}\right)^2 + 4\left(\frac{y+h}{w}\right)^2 - 1\right]}}{2}} \qquad \text{(A-13)}$$

Although $\psi(|x| < w/2,\ y = h)$ should be exactly constant, the approximation is not precise but for simplicity set $\psi(o,h) = V$. Then

$$V = \frac{Q'}{2\pi\varepsilon_o} \sinh^{-1}\left(\frac{4h}{w}\right) \qquad \text{(A-14)}$$

Since $Q' = C'V$, it follows that

$$\frac{\varepsilon_o}{C'} = \frac{L'}{\mu_o} \approx \frac{1}{2\pi} \sinh^{-1}\left(\frac{4h}{w}\right) \qquad \text{(A-15)}$$

When $\varepsilon' > 1$, the situation is more complicated, but the method of images can still be used.

The image pair with dielectric slab of thickness 2h between them shown in Fig. A3a has an E-field within the dielectric that is exactly equivalent to the free space problem with an infinite set of images. The k^{th} set of images is given by $\pm Q'_f(x) \frac{2}{\varepsilon'+1} \left(\frac{\varepsilon'-1}{\varepsilon'+1}\right)^k$. Images for k = 0, 1, and 2 are indicated in Fig. A-3b.

If h/w is large enough so that the noninteracting strip approximation can be made, it follows from superposition and evaluation of $\psi(x=0, y=h) = V$, that

$$\frac{\varepsilon_o}{C'} \simeq \frac{1}{(\varepsilon'+1)\pi} \left\{ \sinh^{-1}\left(\frac{4h}{w}\right) + \sum_{k=1}^{\infty} \left(\frac{1-\varepsilon'}{1+\varepsilon'}\right)^k \left[\sinh^{-1}\left(\frac{4h}{w}(k+1)\right) - \sinh^{-1}\left(\frac{4h}{w}k\right)\right] \right\} . \quad \text{(A-16)}$$

Because by assumption $\frac{h}{w} \geq 1$, the values of

$$\sinh^{-1}\left(\frac{4h}{w}\, n\right) = \ell n \left[\frac{4h}{w}\, n + \sqrt{\left(\frac{4h}{w}\, n\right)^2 + 1}\right] , \quad \text{(A-17)}$$

where n = k or k + 1, can be reasonably approximated as $\ell n\left(\frac{8h}{w}\, n\right)$.

Then

$$\sinh^{-1} \frac{4h}{w}\,(k+1) - \sinh^{-1}\left(\frac{4h}{w}\, k\right) \simeq n\left(1 + \frac{1}{k}\right) \quad \text{(A-18)}$$

and

$$\frac{\varepsilon_o}{C'} \simeq \frac{1}{(\varepsilon'+1)\pi} \left[\sinh^{-1}\left(\frac{4h}{w}\right) + \sum_{k=1}^{\infty} \left(\frac{1-\varepsilon'}{1+\varepsilon'}\right)^k \ell n\left(1 + \frac{1}{k}\right)\right] . \quad \text{(A-19)}$$

Notice that the geometric factor h/W has disappeared from the infinite sum.

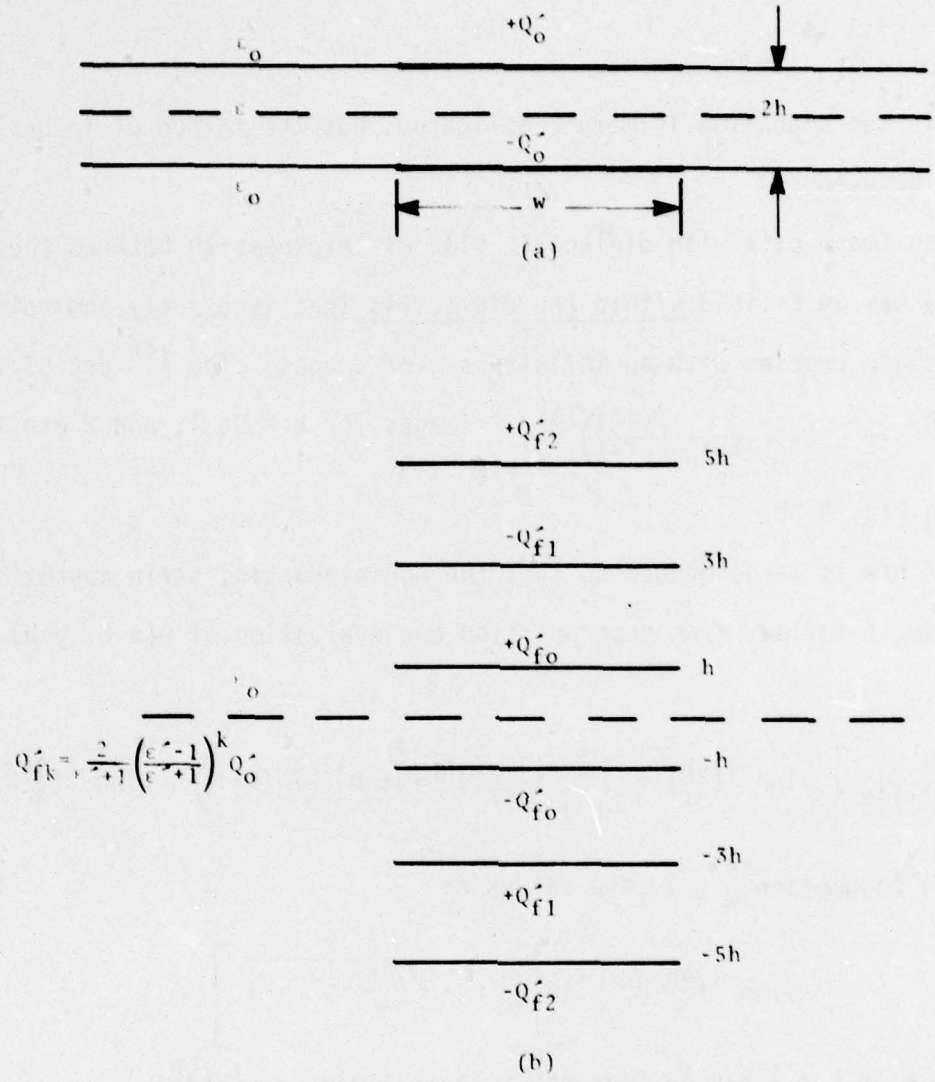

Fields in the upper half of a symmetric structure consisting of a double thickness dielectric slab and a second conducting strip carrying image electric charges, as shown in a, are equivalent to those in Fig. A-1. Insofar as the $\bar{E}$-field inside the dielectric is concerned, the dielectric can be replaced by the image of density Q'_{fk} shown in b.

FIGURE A-3. REPLACEMENT OF MICROSTRIP DIELECTRIC LOADING WITH IMAGE CHARGES

For convenience, we define $\alpha = \frac{\varepsilon'-1}{\varepsilon'+1}$ and since α lies between zero and unity it is possible to approximate the summation with a low-order polynomial. A very simple and quite accurate approximation, is

$$\sum_{k=1}^{\infty} (-\alpha)^K \ln\left(1 + \frac{1}{k}\right) \simeq -\frac{3}{100}\alpha\,(23 - 12\alpha + 4\alpha^2) \equiv \beta(\alpha) \qquad \text{(A-20)}$$

valid for all $0 < \alpha \leq 1$

The final set of equations valid for $\frac{h}{w} \geq 1$ is

$$\frac{L'}{\mu_0} = \frac{1}{2\pi} \sinh^{-1} \frac{(4h)}{w} \qquad \text{(A-21a)}$$

$$\frac{\varepsilon_0}{C'} = \frac{1}{(\varepsilon'+1)\pi} \left[\sinh^{-1} \frac{4h}{w} + \beta\left(\frac{\varepsilon'-1}{\varepsilon'+1}\right)\right] \qquad \text{(A-21b)}$$

These are simple and lend themselves to inversion since

$$\sqrt{\frac{\varepsilon_0}{\mu_0}}\, Z_0 = \sqrt{\left(\frac{L'}{\mu_0}\right)\left(\frac{\varepsilon_0}{C'}\right)} \qquad \text{(A-22)}$$

and

$$\frac{4h}{w} = \sinh\left(\sqrt{\left(2\pi\sqrt{\frac{\varepsilon_0}{\mu_0}}\, Z_0 \frac{\varepsilon'+1}{2}\right)^2 + (\beta/2)^2} - \beta/2\right) \geq 4 \qquad \text{(A-23)}$$

with

$$\beta = -\frac{3}{100}\left(\frac{\varepsilon'-1}{\varepsilon'+1}\right)\left(23 - 12\left(\frac{\varepsilon'-1}{\varepsilon'+1}\right) + 4\left(\frac{\varepsilon'-1}{\varepsilon'+1}\right)^2\right) \qquad \text{(A-24)}$$

Neglecting dispersion, the slowing factor $c/v = \varepsilon'_{eff}$ is again given by Eq. (A-10). Numerical comparison with the published approximate formulas of Wheeler[14] and Hammerstad[16] is very favorable, as shown in Table A-2.

TABLE A-2 NARROW MICROSTRIP

h/w	$\sqrt{\varepsilon'_{eff}}$			$Z_0/\sqrt{\frac{\mu_0}{\varepsilon_0}}$			
	Morgenthaler Eqs. A-21a,b	Wheeler	Hammerstad	Morgenthaler Eqs. A-21a,b	Wheeler	Hammerstad	
1	1		1	.3334	.3350	.3359	
2	1		1	.4419	.4423	.4425	
5	1		1	.5872	.5873	.5873	$\varepsilon' = 1$
10	1		1	.6974	.6975	.6975	
100	1		1	1.0639	1.0639	1.0639	
1	1.2859	1.2837	1.2801	.2593	.2610	.2624	
2	1.2700	1.2701	1.2669	.3479	.3483	.3493	
5	1.2584	1.2589	1.2557	.4666	.4665	.4677	$\varepsilon' = 2$
10	1.2529	1.2534	1.2497	.5567	.5564	.5581	
100	1.2430	1.2434	1.2386	.8859	.8556	.8590	
1	1.8900	1.8799	1.8854	.1764	.1782	.1781	
2	1.8473	1.8450	1.8493	.2392	.2397	.2393	
5	1.8166	1.8165	1.8186	.3232	.3233	.3229	$\varepsilon' = 5$
10	1.8024	1.8027	1.8018	.3869	.3869	.3871	
100	1.7772	1.7778	1.7709	.5986	.5984	.6008	
1	2.5991	2.5792	2.5977	.1283	.1299	.1293	
2	2.5292	2.5234	2.5387	.1747	.1753	.1743	
5	2.4797	2.4781	2.4882	.2368	.2370	.2360	$\varepsilon' = 10$
10	2.4569	2.4563	2.4607	.2839	.2840	.2834	
100	2.4166	2.4169	2.4096	.4402	.4402	.4415	

A.4 QUASI-STATIC COUPLING BETWEEN MICROSTRIP PATCHES

As shown in Fig. A4, consider the two microstrip patches of widths w_1 and w_2 separated by a distance ℓ. The substrate has a dielectric constant ε' and thickness h.

It is well known that the transverse field patterns associated with a TEM mode are Laplacian in character and are therefore identical in form to those generated by dc voltages or dc currents. It is this fact that allows the use of quasi-statics to calculate electric-and magnetic-field coupling coefficients.

A.4.1 ELECTRIC FIELD COUPLING

If the patches are maintained at electrostatic potentials V_1 and V_2 with respect to the ground plane potential $\psi = 0$, the charges (per unit length along z) on the two patches are given by

$$Q_1' = C_{11}' V_1 + C_{12}' V_2 \tag{A-25a}$$

and

$$Q_2' = C_{21}' V_1 + C_{22}' V_2 \tag{A-25b}$$

where the mutual capacitances satisfy $C_{12} = C_{21} < 0$ and it is usual to define a dimensionless coupling coefficient as

$$|k| = \sqrt{\frac{C_{12}' C_{21}'}{C_{11}' C_{22}'}} \quad . \tag{A-26}$$

If $V_2 = 0$ and $h \ll \ell$, it follows that the potential below patch 2 is approximately zero and that above approximately given by Eq. (A1-a).

Since

$$-Q_2' = \varepsilon_o \int_{\ell + w_1/2}^{\ell + w_2 + w_1/2} E_y(x, y = 0+)\, dx \tag{A-27a}$$

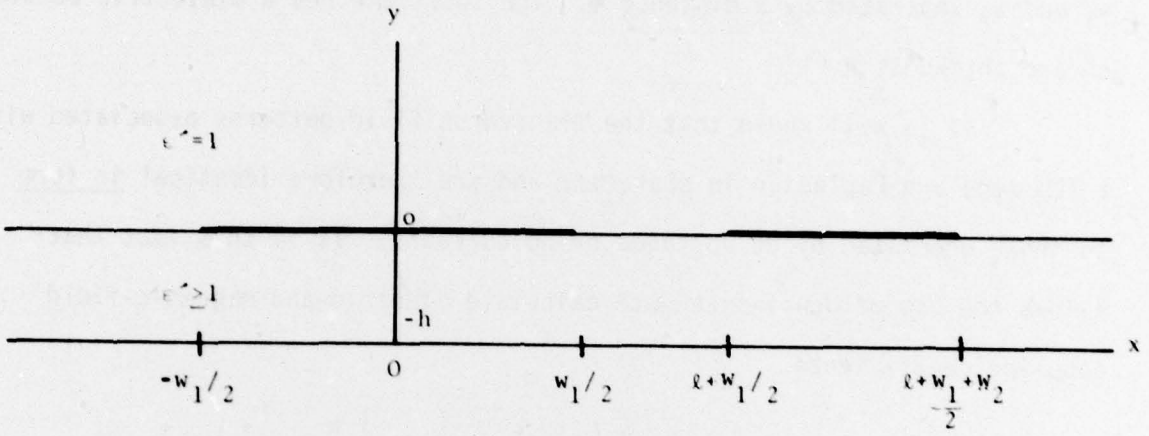

Two microstrip patches of width w_1 and w_2, both spaced a distance h above the same ground plane, parallel to one another and separated by a distance ℓ.

FIGURE A-4. COUPLED MICROSTRIP PATCHES OF FINITE WIDTH

and

$$Q_1' \simeq \varepsilon_o \left[\varepsilon' \frac{V_o}{h} w_1 + \int_{-w_1/2}^{w_1/2} E_y(x, y = 0+)\, dx \right] \qquad \text{(A-27b)}$$

the ratio yields

$$-\left.\frac{Q_2'}{Q_1'}\right|_{V_2=0} = \frac{|C_{21}|}{C_{11}} \simeq \frac{\frac{1}{2\pi p_1} \ln \left[\frac{(\ell + \frac{w_1}{2} + w_2 - p_1) \quad (\ell + \frac{w_1}{2} + p_1)}{(\ell + \frac{w_1}{2} + w_2 + p_1) \quad (\ell + \frac{w_1}{2} - p_1)} \right]}{\frac{\varepsilon'}{h} + \frac{2}{\pi q_1} \tanh^{-1} \left(\frac{w_1/2}{q_1} \right)} \quad . \qquad \text{(A-28)}$$

On the other hand, if $V_1 = 0$,

$$-\left.\frac{Q_1'}{Q_2'}\right|_{V_1=0} = \frac{|C_{12}'|}{C'_{22}} \qquad \text{(A-29)}$$

gives a symmetric formula in terms of an interchange of w_1 and w_2 and p_2, q_2 where

$$p_i = \sqrt{\left(\frac{w_i}{2}\right)^2 - \frac{w_i h}{\pi \varepsilon'}} \quad , \qquad q_i = \sqrt{\left(\frac{w_i}{2}\right)^2 + \frac{w_i h}{\pi \varepsilon'}} \quad .$$

Since $\left(\frac{w_i}{2}\right)^2 >> \frac{w_i h}{\pi \varepsilon'}$, an approximate formula for $|k|$, the coupling coefficient, is

$$|k| \simeq \frac{1}{\pi \sqrt{w_1 w_2}} \frac{\ln \left[\frac{(w_1+\ell)(w_2+\ell)}{(w_1+w_2+\ell)} \right]}{\sqrt{\left[\frac{\varepsilon'}{h} + \frac{2}{\pi w_1} \ln \left(\frac{\pi \varepsilon' w_1}{h} \right) \right] \left[\frac{\varepsilon'}{h} + \frac{2}{\pi w_2} \ln \left(\frac{\pi \varepsilon' w_2}{h} \right) \right]}} << 1 \quad . \qquad \text{(A-30)}$$

A.4.2 MAGNETIC FIELD COUPLING

If magnetostatic fields exist due to z-directed currents i_1 and i_2 flowing in the microstrip patches, the magnetic fluxes per unit length of z, $\Phi_{1,2}$ are related by

$$\Phi_1' = L_{11}' i_1 + L_{12}' i_2 \qquad \text{(A-31a)}$$

and

$$\Phi_2' = L_{-1}' i_1 + L_{22}' i_2 \qquad \text{(A-31b)}$$

where $L'_{12} = L'_{21}$ and $k^2 = \frac{L'_{12}L'_{21}}{L'_{11}L'_{22}}$. An analogous analysis with A_z instead of ψ and $\mu_o A_z = \Phi'$, gives the same formula for $|k|$ as Eq. (A-30) except that ε' is replaced by unity.

The magnetostatic fields near the coupling region when $w_{1,2} >> \ell$ can be described by allowing $w_{1,2} \to \infty$ and using the method of conformal transformation.

For the boundary conditions shown in Fig. (A5), the $\bar{H}$-field can be obtained from $\nabla \times \bar{A}$ where $A_z = Cv$, $\int \bar{H} \cdot d\bar{s} = Cu$ and the conjugate potential functions are related by

$$\frac{\pi(b^2 - 1)x}{2h} = e^u \cos v - 1 + \frac{b^2 - 1}{2} \ell n \left| \frac{e^u}{\sqrt{e^{2u} + 4 - 4e^u \cos v}} \right| \qquad \text{(A-32a)}$$

and

$$\frac{\pi(b^2 - 1)y}{2h} = e^u \sin v + \frac{b^2 - 1}{2} \tan^{-1}\left(\frac{2\sin v}{2\cos v - e^u}\right) . \qquad \text{(A-32b)}$$

The constant b is the solution of the transcendental equation

$$\frac{2b}{b^2 - 1} + \ell n\left(\frac{b+1}{b-1}\right) = \frac{\pi \ell}{2h} \qquad \text{(A-33)}$$

A.4.3 COUPLING BETWEEN $\lambda/4$ RESONANT PATCHES

Reference to Fig. A6a reveals that the mode patterns dictate that magnetic coupling will dominate near the shorted end, whereas electric coupling will dominate near the open circuited end.

Patches oriented as shown in Fig. A6b have very weak H-fields near the open circuited edges, hence, only electric field coupling is important.

In all cases, an increased dielectric constant reduces the fringing E fields, hence, the value of $|k_{electric}|$ by a factor that approaches ε'. (Note that in this case L_1 and L_2 should be used instead of w_1 and w_2 in the coupling formulas.)

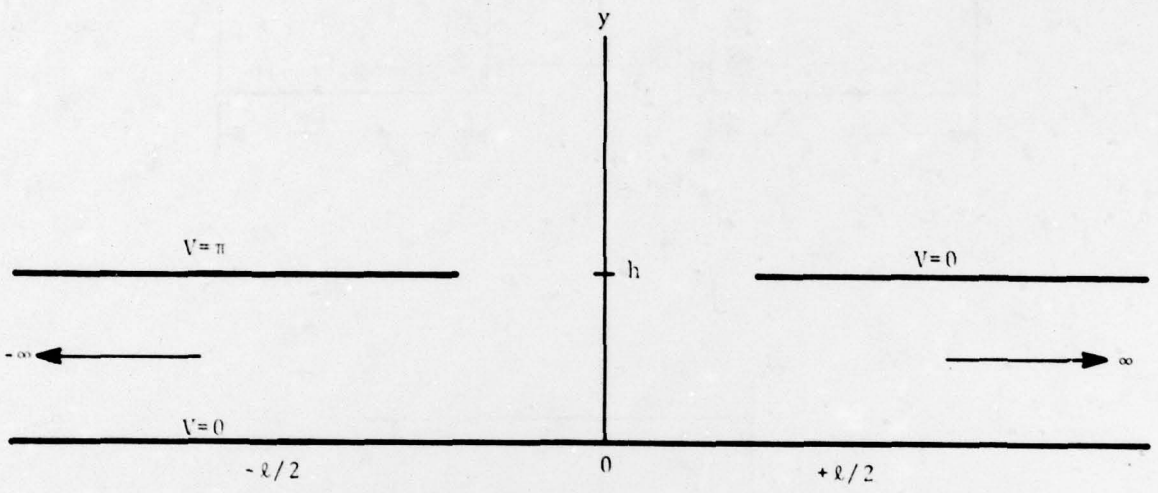

Identical to Fig. A-4, except that $w_1 = w_2 \to \infty$. The static electric and magnetic fields generated by dc charges and currents are solved by the method of conformal mapping.

FIGURE A-5. COUPLED MICROSTRIP PATCHES OF INFINTE EXTENT

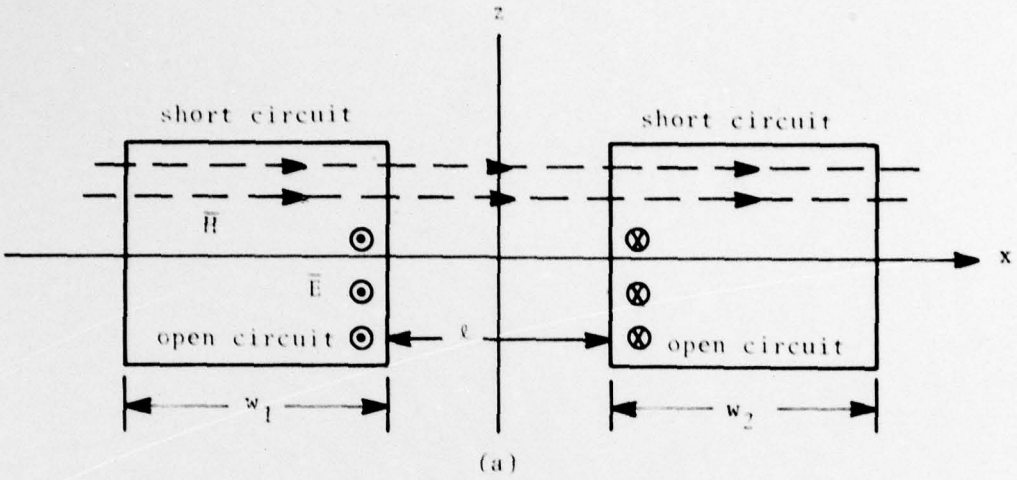

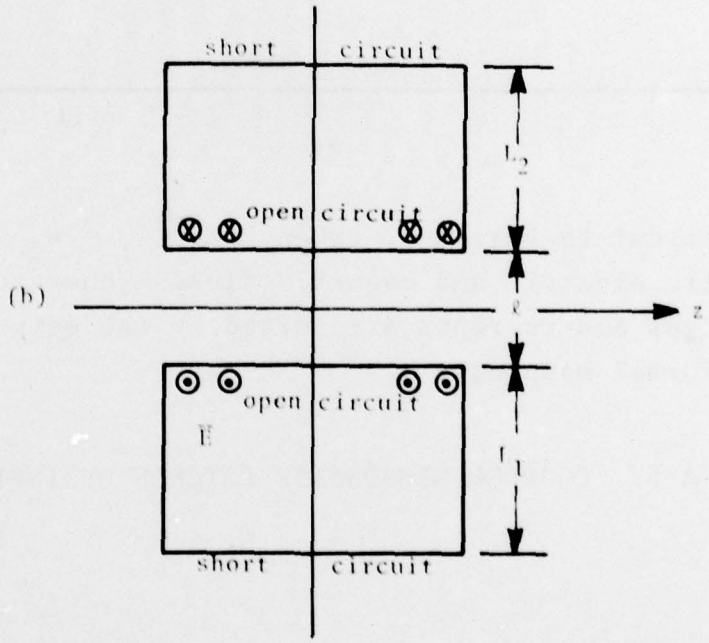

Two rectangular patch microstrip antennas placed either side by side (displaced a distance ℓ along x) or in line (displaced a distance ℓ along z) both electric fields and magnetic fields couple the patches shown in a), whereas it is principally electric fields that couple b). Notice the location of the short circuited edges in b.

FIGURE A-6. COUPLED RECTANGULAR PATCH MICROSTRIP ANTENNAS

Once $|k|$ is known, the amplitude of the mode induced in patch # 2 by a known mode amplitude in patch # 1 can be estimated.

For example, for the case of Fig. (A6b), $Q_2' = 0$, both before and after the voltage V_1 is applied. Therefore, from (A-26)

$$-C_{21}'V_1 + C_{22}'V_2 = 0 \tag{A-34a}$$

$$Q_1' = C_{11}'(1 - k^2)V_1 \tag{A-34b}$$

and

$$V_2(z) = \frac{-C_{21}'}{C_{22}'} V(z) = |k|\sqrt{\frac{C_{11}'}{C_{22}'}}\ V_1(z) \simeq |k| \sqrt{\frac{L_1}{L_2}}\ V_1(z)\ . \tag{A-35}$$

The coupling between patches implies that near resonance, an equivalent circuit can be made, of the type shown in Fig. A7 where mutual inductance M is present, in addition to the coupling capacitance C_c. The transformers model the coupling (via microstrip) into the resonant patches.

If, as is common, the two patches are identical, the coupling splits the degeneracy into closely spaced frequencies.

For circularly polarized arrays, Ball Aerospace Systems Division has developed a crossed-slot element consisting of four $\lambda/4$ microstrip patches arranged as shown in Fig. A-8. The type of analysis outlined above can also be helpful in estimating the coupling coefficients. When known, the level of rf excitation induced on patch # 2 by the level on # 1 (and vice versa), can be estimated. Then the complete $\bar{A}$ and $\bar{A}^*$ can be computed which in turn yield the far-field radiation pattern that includes the effects of the coupling.

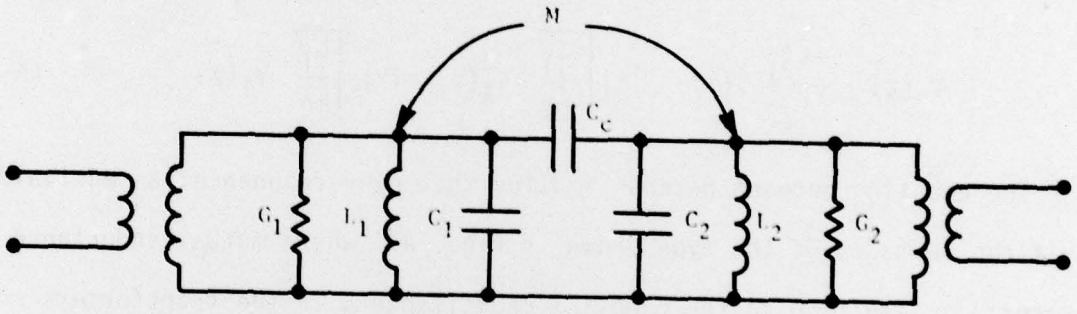

Equivalent circuit governing the coupled resonators of Fig. A-6. The mutal inductance M accounts for the H-field coupling; the capacitance C_c is due to $\bar{E}$-field coupling.

FIGURE A-7. EQUIVALENT CIRCUIT GOVERNING COUPLED RESONATORS

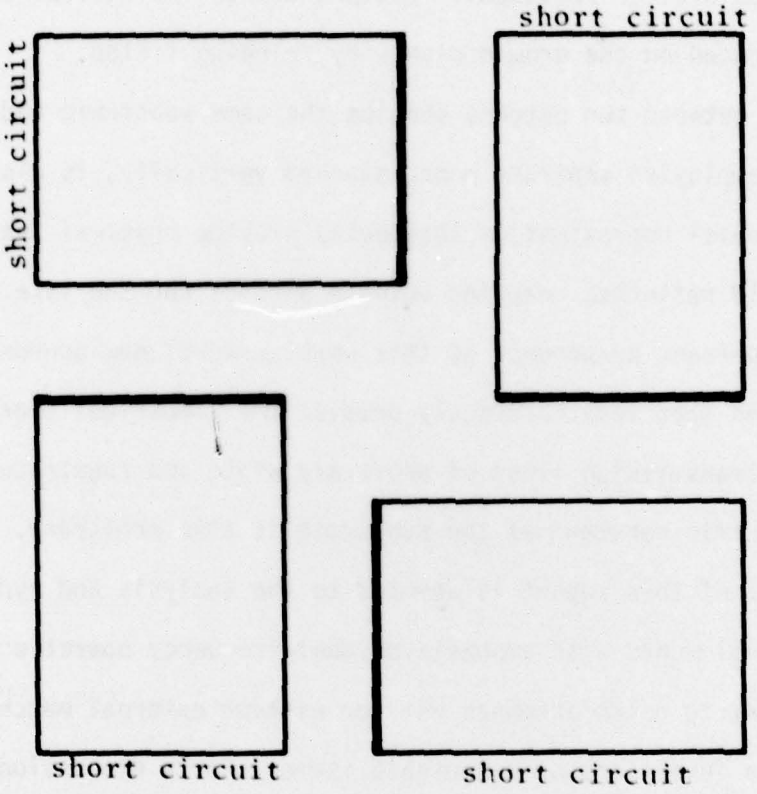

Crossed-slot element consisting of four rectangular microstrip patches. When excited properly, circularly polarized radiation fields are created.

FIGURE A-8. CROSSED-SLOT ELEMENT FOR PRODUCING CIRCULAR-POLARIZED RADIATION

APPENDIX B - REPORT OF NEW TECHNOLOGY

There are no inventions or patentable items contained in Volume I of this report. However, certain advances in the theory of microstrip transmission lines and antennas are reported here.

In particular, for rectangular patch antennas, we include the effects of currents induced on the ground planes by fringing fields.

Coupling between two patches sharing the same substrate and ground plane or else employing separate ones, stacked vertically, is also considered by means of a novel approximation that helps provide physical insight with respect to field patterns, coupling between patches and the like.

As an important by-product of this work, several new approximate formulas are obtained that very accurately predict the electrical characteristics of microstrip transmission lines of arbitrary width and substrate thickness when the dielectric constant of the substrate is also arbitrary.

Volume II of this report is devoted to the analysis and synthesis of multi-resonant elements with emphasis on dual-frequency operation of rectangular microstrip patch antennas with or without external matching networks and may contain inventions or patentable items. For a discussion, please refer to the appendix of Vol. II of this report.

220 copies

REFERENCES

1. Deschamps, Georges A., "Microstrip microwave antennas," presented at the 3rd USAF Symposium, 1953.

2. Munson, R.E., "Conformal microstrip antennas and microstrip phased arrays," IEEE Trans. Antennas Propagat., vol. AP-22, no. 1, January 1974, pp. 74-78.

3. Itoh, T. and R. Mittra., "Analysis of microstrip disk resonator," Arch. Elek. Übertragung., vol. 27, November 1973, pp. 546-458.

4. Sanford, G., "Conformal Microstrip Phased Array for Aircraft Tests with ATS-6, "Proceedings of the National Electronics Conference, Vol. XXIX, 1974, pp. 252-257.

   1979 Final Report, DOT-TSC-1397, in preparation.

5. Weinschel, D. "A cylindrical array of circularly polarized microstrip antennas," 1975 AP-S International Synposium (p. 177 of Digest).

6. Sanford, G. and L. Klein, "Development and Test of a Conformal Microstrip Airborne Phased Array for Use with the ATS-6 Satellite," IEE Conference Publication No. 128, 1975.

   "Recent Developments in the Design of Conformal Microstrip Phased Arrays," International Conference on Maritime and Aeronautical Satellite Communication and Navigation, March 7-9, 1978, IEE Savoy Place, London WC2.

7. Howell, J.Q., "Microstrip Antennas," IEEE Trans. Antennas Propagat. (1975) AP-23: 90-93.

8. Agrawal, P.K. and M.C. Bailey, "An analysis technique for microstrip antennas," IEEE Society of Antennas Propagat. Int. Symp. (1976) PP. 395-398.

9. Derneryd, A.G., "Linearly polarized microstrip antennas," IEEE Trans. Antennas Propagat. (1976), AP-24: 846-851.

   "A theoretical investigation of the rectangular microstrip antenna element," RADC-TR-77-206 (1977).

   "Analysis of the microstrip disk antenna element," RADC-TR-383 (1977).

10. Lo, Y.T. and G.A. Deschamps, "Study of microstrip antennas, microstrip phased arrays, and microstrip feed networks," Quarterly Report No. 1, Feb. 2, 1976 - May 1, 1976.

REFERENCES (CONT.)

11. James, J.R. and G.J. Wilson, "Microstrip antennas and arrays. Pt.-1 - Fundamental action and limitations," Microwave, Optics, and Acoustics, Vol. 1, #5, Sep 1977, pp. 165-174.

James, J.R. and P.S. Hall, "Microstrip antennas and arrays. Pt.-2 - New array-design technique," Microwave, Optics and Acoustics, Vol. 1, #5, Sep 1977, pp. 175-181.

12. Chu, L.J. "Electromagnetic Fields, Energy and Forces," Appendix One, John Wiley (1960).

13. James, J.R., "Surface-Wave Phenomena Associated with Open-Circuited Stripline Terminations," Electronics Letters, 29 November 1973, 9, No. 24, pp. 570-571.

14. Wheeler, H.A., "Transmission-Line Properties of a Strip on a Dielectric Sheet on a Plane," IEEE Trans. Vol. MTT-25, pp. 631-647 (1977).

"Stripline (Microstrip) Analysis, Synthesis and Loss," Hewlett-Packard Users Library Program 01738D.

15. Schneider, M.W., "Microstrip Lines for Microwave Integrated Circuits," Bell System Tech. Journ. May-June 1969, pp. 1421-1443.

16. Hammerstad, E.O., and F. Beckkadal, "Microstrip Handbook." ELAB report STF 44A74169, University of Trondheim, Norway, 1975, pp. 98-110.

Hammerstad, E.O., "Microstrip Handbook." ELAB report STF 44A74169, University of Trondheim, Norway, A75, pp. 98-110.

17. Kwon, A.H., "Design of Microstrip Transmission Line," Microwave Journal, Application Note, p. 61, Jan. 1976.

220 copies